JOURNAL OF GEOPHYSICAL RESEARCH, VOL. 112, B10308, doi:10.1029/2006JB004847, 2007

Seismically and geodetically determined nondouble-couple source mechanisms from the 2000 Miyakejima volcanic earthquake swarm

Sarah E. Minson,[1] Douglas S. Dreger,[2] Roland Bürgmann,[3] Hiroo Kanamori,[4] and Kristine M. Larson[5]

Received 9 November 2006; revised 24 May 2007; accepted 4 June 2007; published 25 October 2007.

[1] The volcanic eruption on Miyakejima, Japan, in 2000 was marked by the largest earthquake swarm ever recorded in Japan, a seismicity migration accompanying a dike intrusion as the dike propagated from Miyakejima to the northwest, and formation of a caldera on Mount Oyama on Miyakejima. In this study, we propose a seismic source model which can be used to model both seismic and geodetic displacements from volcanic earthquakes. Our model, the "crack + double-couple" (CDC) model, combines tensile opening with shear slip along a single fault plane. We find that this model can fit both seismic and GPS data from the 1 July and 30 July earthquakes, the largest two in the Miyakejima sequence. The results of our GPS inversions for these two earthquakes are consistent with the seismic mechanisms and aftershock locations, and the GPS mechanisms successfully forward predict the observed regional seismograms. The 1 July earthquake, located near the northwest tip of the dike, has a large opening component and a geodetic moment about 5 times larger than that inferred from the seismic data alone. The source process for this event consists of tensile failure, which occurred quickly, and a much slower accumulation of shear slip. We apply the CDC model to 16 additional earthquakes from this sequence and find that the CDC model fits the seismic data for these earthquakes at least as well as established seismic moment tensor models.

Citation: Minson, S. E., D. S. Dreger, R. Bürgmann, H. Kanamori, and K. M. Larson (2007), Seismically and geodetically determined nondouble-couple source mechanisms from the 2000 Miyakejima volcanic earthquake swarm, *J. Geophys. Res.*, *112*, B10308, doi:10.1029/2006JB004847.

1. Introduction

[2] The 2000 Miyakejima volcanic eruption and offshore dike intrusion were accompanied by many anomalous earthquakes with source mechanisms containing large nondouble-couple components (Figure 1). The eruptive sequence in the Izu volcanic islands more than 150 km south of Tokyo was marked by both substantial crustal deformations and an earthquake swarm which included many magnitude 5 and larger earthquakes. These earthquakes were recorded by local and regional seismic and GPS networks. This provides a unique opportunity to use both seismic and GPS data to learn about the source processes of nondouble-couple earthquakes.

[3] In this study, we have used several seismic and GPS inversion methods to investigate the source processes of 18 earthquakes: the twelve events in the sequence with moment magnitudes of at least 5.5 as well as six smaller earthquakes which preliminary F-net Broadband Seismograph Network automated moment tensors identified as having anomalous source mechanisms (available at http://www.fnet.bosai.go.jp/freesia/event/hypo/joho.html). A useful metric for whether a source mechanism is anomalous is the ε value [*Dziewonski et al.*, 1981]. Let m_1^*, m_2^*, and m_3^* be the eigenvalues of a deviatoric moment tensor (i.e., a symmetric moment tensor with vanishing trace) with the convention $|m_1^*| \geq |m_2^*| \geq |m_3^*|$. Then ε is defined by the ratio of $|m_3^*|$ to $|m_1^*|$, i.e.,

$$\varepsilon = \left|\frac{m_3^*}{m_1^*}\right| for |m_1^*| \geq |m_2^*| \geq |m_3^*| \quad (1)$$

For a double-couple source, $\varepsilon = 0$, and $\varepsilon = 0.5$ if the deviatoric part of the mechanism is completely nondouble-couple; that is, if the deviatoric component is a compensated linear vector dipole (CLVD) [*Knopoff and Randall*, 1970].

[1]Department of Geological and Planetary Sciences, California Institute of Technology, Pasadena, California, USA.
[2]Department of Geology and Geophysics, University of California, Berkeley, California, USA.
[3]Department of Earth and Planetary Science, University of California, Berkeley, California, USA.
[4]Seismological Laboratory, California Institute of Technology, Pasadena, California, USA.
[5]Department of Aerospace Engineering Sciences, University of Colorado, Boulder, Colorado, USA.

0148-0227/07/2006JB004847$09.00

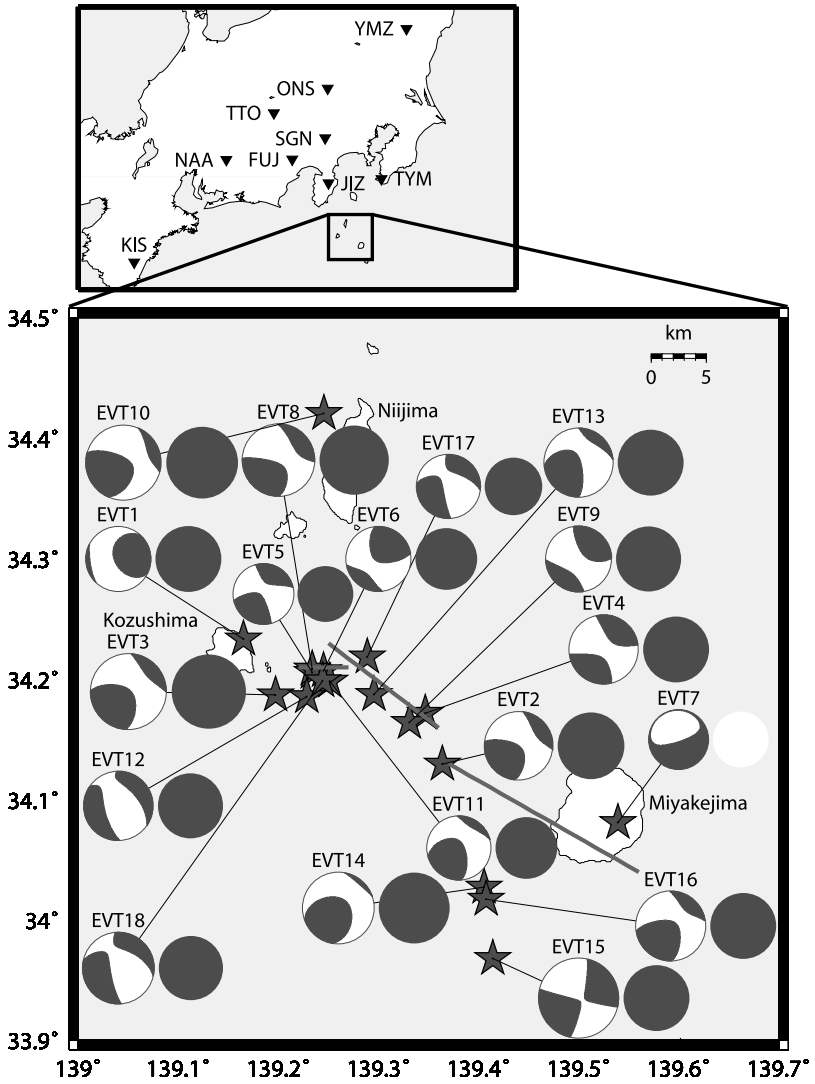

Figure 1. Map showing locations and CDC solutions for the 18 earthquakes in this study. The CDC mechanisms are decomposed into deviatoric and isotropic components. Triangles mark the locations of F-net Broadband Seismograph Stations. Gray lines indicate the dike geometry from *Furuya et al.* [2003].

A comparison of the ε values from the Harvard centroid moment tensor (CMT) catalog, which lists source mechanisms determined from deviatoric moment tensor inversions, to our deviatoric mechanisms for the Miyakejima earthquakes, shows that the Miyakejima sequence has an unusually large number nondouble-couple events (Figure 2). In order to explain these anomalous source mechanisms we must find a physically realistic nondouble-couple source model and derive a seismic moment tensor representation of that source model. In particular, we focus on the two largest events, M_w 6.2 EVT3 on 1 July and M_w 6.4 EVT15 on 30 July (Table 1), for which the observed GPS displacements provide valuable complementary information about the kinematic expression of the events.

2. Miyakejima Eruption and Dike Intrusion

[4] Mount Oyama on Miyakejima is located in the northern Izu-Bonin volcanic arc on the Philippine Sea plate. At the Izu Peninsula triple junction, the Philippine Sea plate is underthrust by the Pacific plate at approximately 10 cm/yr as it subducts to the northwest under Japan at approximately 4 cm/yr [e.g., *Apel et al.*, 2006; *Seno et al.*, 1993; *Zang et al.*, 2002]. Since 1940, Mount Oyama has erupted approximately every twenty years. Its most recent period of unrest began on 26 June 2000 with the initiation of the largest earthquake swarm ever recorded in Japan, including more than six hundred earthquakes of magnitude 4.0 and greater [*Japan Meteorological Agency* (*JMA*), 2000; *Ito and Yoshioka*, 2002]. The seismicity was observed to migrate to the northwest toward Kozushima with the inferred emplacement of a dike [*JMA*, 2000]. This was accompanied by caldera collapse on Miyakejima and at least one offshore eruption. Significant dike inflation is confirmed by large displacements of GPS sites on the islands, which indicate a dike volume increase of more than 1 km^3 during the 2-month-long period [*Nishimura et al.*, 2001; *Toda et al.*, 2002; *Ozawa et al.*, 2004]. The dike intrusion was fed by a magma source beneath Miyakejima, and pos-

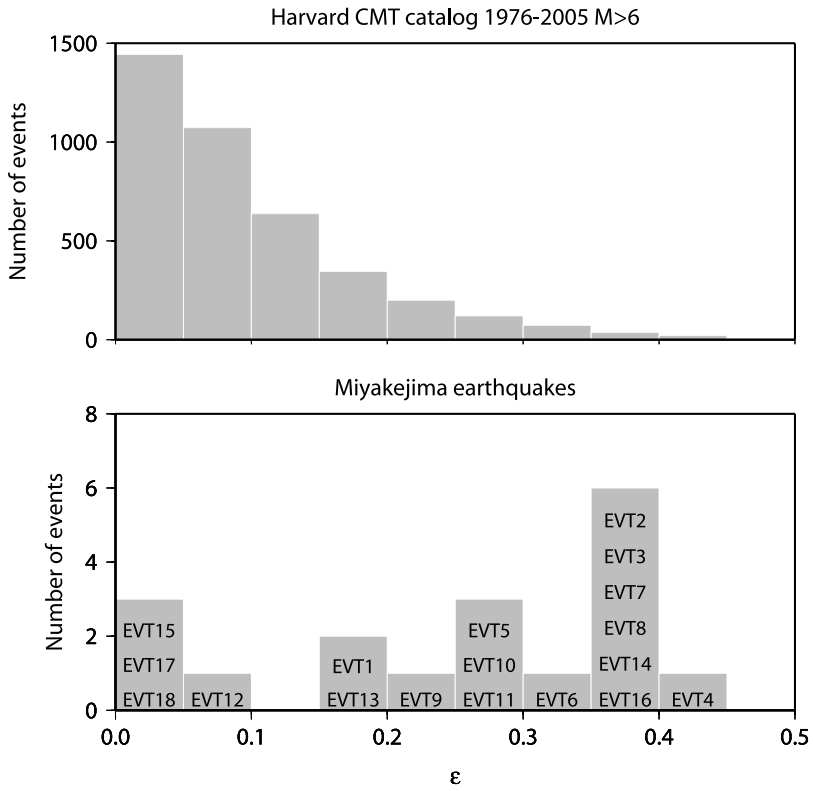

Figure 2. Comparison of ε values for the cumulative Harvard CMT catalog to those of the deviatoric moment tensor mechanisms from this study. The distribution of ε values for the Miyakejima earthquakes show that a much greater number of them have large nondouble-couple components than is seen in the global earthquake distribution.

sibly by an additional source near Kozushima as well [*Furuya et al.*, 2003].

3. Moment Tensor Decomposition

[5] Most earthquakes are well described by the double-couple (DC) source model consistent with slip on a planar fault surface. (This is equivalent to requiring the seismic moment tensor to be deviatoric with $|m_1^*| = |m_3^*|$, and $|m_2^*| = 0$.) However, in volcanic settings, where volumetric deformation is common, nondouble-couple mechanisms are often observed [e.g., *Julian and Sipkin*, 1985; *Julian et al.*, 1997; *Dreger et al.*, 2000] and some earthquakes may have more complicated mechanisms. Full moment tensor (FMT) inversions can, in theory, recover any seismic source with the exception of a single force. In FMT inversions, all six unique elements of the symmetric seismic moment tensor are free parameters. However, these inversions can have large

Table 1. JMA Hypocenter Information for the Earthquakes in This Study

Event	Date	Origin Time, UT	Latitude	Longitude	Depth, km	Magnitude M_J
EVT1	2000/6/29	0311:52.50	34.23367	139.16500	11.94	5.2
EVT2	2000/6/29	0630:23:20	34.12983	139.36383	19.04	5.6
EVT3	2000/7/1	0701:56.30	34.18717	139.19700	16.07	6.4
EVT4	2000/7/2	2003:36.60	34.17200	139.34683	16.16	5.4
EVT5	2000/7/6	1859:37.50	34.20600	139.23383	17.31	4.9
EVT6	2000/7/7	0245:28.20	34.20717	139.24517	16.57	5.0
EVT7[a]	2000/7/8	0941:45.38	34.08137	139.53866	0.883	3.7
EVT8	2000/7/8	1857:44.90	34.20883	139.23367	15.39	6.1
EVT9	2000/7/14	1828:24.20	34.16450	139.33100	14.66	5.2
EVT10	2000/7/15	0130:32.00	34.42050	139.24533	9.56	6.3
EVT11	2000/7/20	0310:26.20	34.19867	139.25117	15.35	5.1
EVT12	2000/7/23	2152:45.80	34.18583	139.22817	11.67	5.5
EVT13	2000/7/27	0149:53.30	34.18750	139.29550	12.73	5.6
EVT14	2000/7/30	0018:02.20	34.02733	139.40533	11.17	5.8
EVT15	2000/7/30	1225:46.60	33.96800	139.41433	17.10	6.5
EVT16	2000/7/30	1248:57.10	34.01750	139.40733	16.81	5.7
EVT17	2000/8/2	2142:27.60	34.21867	139.28883	15.47	5.1
EVT18	2000/8/18	0152:22.60	34.19900	139.24433	12.38	6.0

[a]Relocated by S. Sakai.

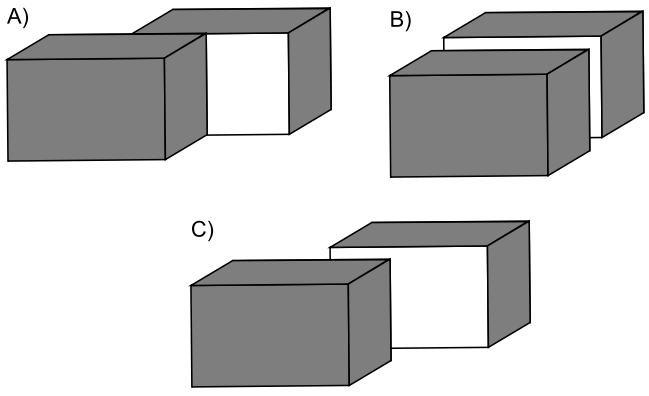

Figure 3. Kinematics of the CDC moment tensor decomposition. The CDC model combines (a) a shear fault with (b) a crack opening perpendicular to that fault plane. (c) This decomposition results in a mechanism which is composed of both shearing and opening.

Table 2. Tokai Velocity Model Used to Calculate Green's Functions[a]

Thickness, km	P Wave Velocity, km/s	S Wave Velocity, km/s	Density, kg/m^3	Q_α	Q_β
3.0	5.50	3.14	2300	600	300
15.0	6.00	3.55	2400	600	300
15.0	6.70	3.83	2800	600	300
67.0	7.80	4.46	3200	600	300
—	8.00	4.57	3300	600	300

[a]See *Fukuyama and Dreger* [2000].

trade-offs between moment tensor elements or contain nonphysical source parameters such as multiple compensating volumetric components [*Dufumier and Rivera*, 1997].

[6] In order to stabilize and constrain moment tensor inversions, source mechanisms are commonly assumed to be deviatoric, reducing the number of independent moment tensor elements to five. (Harvard CMT solutions; University of California, Berkeley, regional moment tensors; Southern California Seismic Network moment tensors; and F-net Broadband Seismograph Network moment tensors are all deviatoric moment tensor solutions.) Deviatoric solutions assume that the source has no net volume change and the trace of the moment tensor is zero. However, the deviatoric source model does not allow for a volumetric source component, which has been observed in volcanic seismicity. Furthermore, there is no straightforward kinematic interpretation of the nondouble-couple component of deviatoric mechanisms. Without a kinematic interpretation, we cannot construct mechanically meaningful source models which are consistent with our seismic modeling and which can be used to model geodetic surface displacements.

[7] Sources which contain a volumetric component can be modeled by a combination of shear (double-couple, DC) slip and an isotropic (ISO) volume change. This model, referred to as DC + ISO, also has only five independent moment tensor elements. It has been used in several studies of volcanic source mechanisms and nuclear explosions [e.g., *Dreger and Woods*, 2002; *Templeton and Dreger*, 2006]. While DC + ISO solutions for nuclear detonations can be explained as tectonic (double-couple) release triggered by the (isotropic) explosion, there is no obvious kinematic interpretation of DC + ISO solutions for natural seismic events. In this study, we consider another constrained source model in which it is assumed that the source mechanism is a combination of shear (double-couple) slip and a tensile crack for which the opening direction is normal to the shear plane (Figure 3). This is simply a special case of the *Dufumier and Rivera* [1997] moment tensor decomposition. Our model, called the "crack + double-couple" model or CDC model, introduces a constraint on the form of the moment tensor which reduces the number of free parameters to five (strike, dip, rake, double-couple moment, tensile moment) and does not allow for multiple compensating volumetric components.

4. CDC Model

[8] As discussed above, we interpret the nondouble-couple earthquakes of the Miyakejima sequence as a combination of a shear fault and a tensile crack which opens in the direction normal to the fault plane. The equivalent force system for a tensile crack involves net volume change. This is in contrast to the CLVD (compensated linear vector dipole [*Knopoff and Randall*, 1970]) model which involves no volume change. CLVDs are often used to model earthquakes in volcanic areas [e.g., *Julian and Sipkin*, 1985]. A tensile crack and CLVD are similar in that both represent an opening crack, but in the CLVD model it is implicitly assumed that material flows rapidly into the opening crack from the nearby area so that no net volume change is involved. However, this flow may not occur very rapidly in viscous magma and, on the timescale of seismic radiation, a tensile crack model with net volume change may be more appropriate. Also, it is possible that injection may involve net volume change as is postulated by *Kanamori et al.* [1993] for the 1984 Torishima, Japan, earthquake.

[9] *Kanamori et al.* [1993] argue that the duration of the source time function is too short for magma to propagate across the length of the source region. Thus the earthquake must have resulted from the interaction of magma with water rather than the injection of magma alone. Magma would tend to heat any water present, increasing the water's volume. This occurs gradually and does not radiate seismically. Eventually, the water becomes a supercritical fluid whose pressure exceeds the failure strength of the surrounding medium, leading to rapid hydrofracturing-type failure, and creating a net volume change. It is this rapid failure process which radiates seismically. Thus the tensile part of the seismic source process is not compensated, and is not a CLVD. With these considerations, we prefer the CDC model to the CLVD model for interpretation of the Miyakejima sequence.

[10] The CDC model is the superposition of shear and tensile dislocations [*Okada*, 1985, after *Mansinha and Smylie*, 1971] normally used in geodetic inversions of seismic sources. Thus we can use a CDC moment tensor to calculate static surface displacements for a nondouble-couple volcanic source. Also, we can use the results of a

Table 3. Variance Reduction for All of the Events Studied and Source Depths Determined From Deviatoric Moment Tensor Inversions[a]

Event	Depth, km	DC	Deviatoric	DC + ISO	CDC	FMT
EVT1	2	62.51	63.80	65.85	65.98	66.40
EVT2	4	83.91	85.46	86.84	86.72	86.75
EVT3	4	84.96	88.04	87.79	88.43	88.62
EVT4	4	88.55	90.23	89.76	90.44	90.97
EVT5	6	84.81	87.40	86.91	86.48	87.86
EVT6	4	84.86	87.33	87.39	87.43	88.12
EVT7	4	43.23	55.07	65.80	62.78	67.57
EVT8	4	87.10	88.86	89.85	89.63	89.83
EVT9	4	87.07	89.87	87.99	89.15	90.05
EVT10	4	87.92	90.14	90.78	91.29	91.26
EVT11	2	91.07	91.71	91.43	91.49	92.04
EVT12	4	78.14	80.55	79.10	78.50	81.03
EVT13	2	88.32	88.77	88.32	88.63	88.97
EVT14	2	86.58	87.37	87.90	88.17	88.18
EVT15	10	86.97	86.96	87.26	87.04	87.46
EVT16	4	86.18	87.23	88.14	87.87	88.29
EVT17	2	86.18	86.24	86.27	86.23	86.42
EVT18	2	85.61	85.84	86.04	85.93	86.08

[a]The variance reduction (in%) (VR) is defined as $VR = \{1.0 - [\int(\text{data} - \text{synthetic})^2\, dt]/[\int(\text{data})^2\, dt]\}100\%$. The values are from moment tensor inversions of data passband filtered between 20 and 50 s period.

Table 4. Double-Couple Solutions for Miyakejima Earthquakes[a]

	T Axis			I Axis			P Axis		
Event	Value	Trend	Plunge	Value	Trend	Plunge	Value	Trend	Plunge
EVT1	101.0	73.2	22.4	0	−23.8	16.6	−101.0	−147.3	61.6
EVT2	245.7	−129.5	3.6	0	137.0	44.7	−245.7	−35.9	45.1
EVT3	1775.0	−135.9	8.3	0	126.3	42.8	−1775.0	−37.2	46.0
EVT4	328.8	−145.1	0.4	0	124.5	44.5	−328.8	−54.7	45.5
EVT5	26.3	−145.6	11.7	0	−39.8	52.9	−26.3	116.2	34.6
EVT6	77.0	33.4	13.4	0	−75.8	54.1	−77.0	132.2	32.6
EVT7	42.4	−56.7	14.2	0	35.9	10.4	−42.4	160.9	72.3
EVT8	662.6	−134.7	1.8	0	133.7	42.3	−662.6	−42.7	47.6
EVT9	154.3	43.0	9.2	0	138.0	28.1	−154.3	−63.4	60.1
EVT10	1118.0	−118.8	9.1	0	135.6	59.4	−1118.0	−23.7	29.0
EVT11	59.0	−138.6	18.4	0	−28.0	46.6	−59.0	116.5	37.6
EVT12	324.8	−117.7	7.4	0	−25.8	14.5	−324.8	126.0	73.7
EVT13	263.4	−127.9	23.0	0	−18.6	38.0	−263.4	118.6	43.2
EVT14	341.9	−143.7	15.0	0	106.0	52.3	−341.9	−43.4	33.6
EVT15	4655.0	−123.1	4.3	0	120.5	80.5	−4655.0	−32.5	8.5
EVT16	283.7	−143.9	13.8	0	102.2	58.8	−283.7	−46.6	27.4
EVT17	65.6	−129.0	15.0	0	−24.6	42.8	−65.6	126.3	43.4
EVT18	480.5	−128.2	8.4	0	−30.9	40.7	−480.5	132.4	48.1

[a]Eigenvalues are given in 10^{15} N m. Trend and plunge are given in degrees clockwise from north and degrees below horizontal, respectively. The intermediate eigenvalues of DC solutions are zero by definition.

geodetic source inversion to forward predict observed seismograms.

5. Moment Tensors From Seismic Data

[11] We have modeled 18 earthquakes (Table 1) using broadband seismograms recorded at stations in the F-net Broadband Seismograph Network, and for each event we investigated five different source models: DC, deviatoric, FMT, DC + ISO, and CDC. (The CDC moment tensor decomposition is discussed in detail in Appendix A.) Although the F-net stations are all located to the north of the earthquakes in this study (Figure 1), the results of our deviatoric moment tensor inversions are nearly identical to the Harvard CMT solutions which use a global distribution of stations at teleseismic distances. Thus our results do not appear to be biased by either our station geometry or the local velocity structure. Furthermore, the source-receiver distances are much greater than the distances between individual earthquakes in this study, some of which do appear to have double-couple mechanisms. This indicates that there is no systematic bias toward nondouble-couple solutions due to any complex propagation effects.

[12] To determine the deviatoric and FMT solutions, we used a corrected (S. E. Minson and D. S. Dreger, Stable inversions for complete moment tensors, submitted to *Geophysical Journal International*, 2007) form of the linear time domain moment tensor inversions employed by *Dreger et al.* [2000] and *Dreger and Woods* [2002]. Although we assumed that the reported latitude and longitude of the hypocenters are correct, we repeated deviatoric inversions for depths from 2 km to 16 km in increments of 2 km. Whichever depth yielded the best fit to the data was assumed to be correct, and we used that depth in all of our source modeling. As the DC, DC + ISO and CDC (see the appendix) constraints on the moment tensor are nonlinear, a grid search approach was used to determine the respective source parameters. For example, a CDC mechanism is uniquely determined by five parameters: strike, dip, rake, double-couple moment, and tensile

Table 5. Deviatoric Solutions for Miyakejima Earthquakes[a]

	T Axis			I Axis			P Axis		
Event	Value	Trend	Plunge	Value	Trend	Plunge	Value	Trend	Plunge
EVT1	84.2	81.6	13.2	−14.9	−9.0	2.6	−69.2	−109.9	76.6
EVT2	264.2	−128.2	12.5	−102.3	133.8	32.3	−161.9	−19.9	54.8
EVT3	2074.0	−133.4	18.8	−781.4	−37.1	17.9	−1293.0	93.4	63.6
EVT4	325.8	−148.2	3.4	−143.0	119.1	38.9	−182.9	−54.0	50.9
EVT5	28.8	−150.6	11.4	−7.6	−35.2	64.8	−21.2	114.7	22.2
EVT6	87.3	34.2	16.6	−29.2	−121.9	72.0	−58.1	126.2	6.9
EVT7	66.2	48.5	32.7	38.1	−45.8	6.7	−104.3	−146.0	56.4
EVT8	715.1	−135.7	11.7	−285.8	130.1	19.4	−429.3	−16.2	67.1
EVT9	154.6	37.1	5.8	−35.1	−53.8	8.4	−119.5	161.1	79.8
EVT10	1486.0	−119.1	21.1	−410.9	126.4	47.1	−1075.0	−13.2	35.3
EVT11	63.6	−143.0	21.5	−17.6	−21.9	52.6	−46.0	114.4	28.9
EVT12	386.3	−110.5	19.4	21.2	−15.4	14.1	−407.5	108.3	65.7
EVT13	298.3	−130.1	27.7	−46.6	−21.1	31.8	−251.7	107.7	45.4
EVT14	463.4	−142.4	28.0	−183.2	100.9	40.2	−280.2	−28.8	37.0
EVT15	4334.0	−124.1	6.8	120.7	107.9	79.1	−4455.0	−33.1	8.5
EVT16	341.8	−141.9	22.2	−129.8	62.5	65.8	−212.1	−48.2	9.0
EVT17	66.2	−127.9	16.6	0.0	−22.7	41.2	−66.3	125.4	44.1
EVT18	544.4	−123.5	19.5	3.4	−20.0	33.4	−547.8	121.6	50.0

[a]Eigenvalues are given in 10^{15} N m. Trend and plunge are given in degrees clockwise from north and degrees below horizontal, respectively.

Table 6. DC + ISO Solutions for Miyakejima Earthquakes[a]

	T Axis			I Axis			P Axis		
Event	Value	Trend	Plunge	Value	Trend	Plunge	Value	Trend	Plunge
EVT1	163.1	78.7	47.6	102.8	−97.7	42.3	42.5	170.7	1.8
EVT2	323.9	−129.4	20.9	121.4	75.2	67.2	−81.0	−36.1	8.6
EVT3	2345.0	−134.8	21.0	959.5	58.5	68.5	−426.4	−43.1	4.5
EVT4	362.4	35.3	0.1	120.8	125.7	77.3	−120.8	−54.7	12.7
EVT5	31.7	−147.7	16.8	8.0	3.8	71.1	−15.7	119.7	8.5
EVT6	116.3	34.4	29.5	36.3	−128.9	59.4	−43.6	128.6	7.3
EVT7	145.8	46.2	53.6	64.8	−51.9	5.9	−16.2	−146.2	35.7
EVT8	903.2	−135.7	19.0	357.6	74.8	68.2	−187.9	−42.1	10.3
EVT9	198.5	42.9	16.5	85.6	168.1	62.9	−27.2	−53.6	21.0
EVT10	1825.0	−119.7	35.0	608.3	76.5	54.0	−608.3	−24.2	7.7
EVT11	105.8	−142.4	43.7	46.8	32.0	46.1	−12.1	124.9	2.8
EVT12	357.2	−114.5	12.1	95.3	−17.5	29.8	−166.7	136.0	57.4
EVT13	316.3	−128.3	30.0	96.3	1.5	47.9	−123.8	124.9	26.5
EVT14	753.6	−144.9	52.3	353.2	46.9	37.2	−47.1	−47.5	5.7
EVT15	5053.0	−123.1	4.3	219.7	120.5	80.5	−4614.0	−32.5	8.5
EVT16	459.7	−141.5	39.8	155.1	45.9	50.0	−149.6	−48.5	3.7
EVT17	65.4	−129.5	12.8	2.3	−26.3	45.2	−60.8	128.7	42.0
EVT18	618.9	−125.2	17.6	169.3	−14.1	48.7	−280.3	131.5	36.0

[a]Eigenvalues are given in 10^{15} N m. Trend and plunge are given in degrees clockwise from north and degrees below horizontal, respectively.

moment. After an initial coarse grid search to determine rough estimates for the moments, we determine a final solution from a fine grid search. These fine grid searches test all possible values for strike, dip, and rake in increments of three degrees; and test ten values each for double-couple moment and tensile moment. The mechanism with the best fit to the data is chosen as the solution. Green's functions for the moment tensor inversions were calculated using frequency wave number integration [*Saikia*, 1994] for a one-dimensional velocity structure (Table 2). The data and Green's functions were band-pass filtered between periods of 20 and 50 s.

[13] The results for all inversions are listed in Tables 3–10. All of the models that were tested fit the data quite well, making it difficult to discriminate between models (Figure 4). For most events studied, a model with a net volume change (DC + ISO, CDC, or FMT) is preferable to a deviatoric model. Three events (EVT15, EVT17 and EVT18) are clearly double-couple (Figure 2), and EVT7 stands out as being distinctly different from the other events in terms of the level of fit attainable and the difference in fit between the different source mechanisms.

[14] Sample waveform fits for the EVT3 CDC solution are presented in Figure 5. In Figure 6, we plot the assemblage of CDC mechanisms which fit the EVT3 data with a variance reduction within 5% of the value from the best fit mechanism. This demonstrates that the CDC mechanism for EVT3 is quite stable and well constrained while Figure 5 shows that the CDC mechanism fits the data quite well.

[15] Figure 4 shows only a small increase in variance reduction for the FMT solutions relative to the various five parameter models (deviatoric, DC + ISO, and CDC). So it does not appear that the data require an unconstrained full moment tensor solution. However, we see a larger increase in variance reduction for the five parameter models (deviatoric, DC + ISO, and CDC) relative to the simpler double-couple model. We argue that the CDC model is preferable for most of the events not because of a large improvement in

Table 7. CDC Solutions for Miyakejima Earthquakes[a]

	T Axis			I Axis			P Axis		
Event	Value	Trend	Plunge	Value	Trend	Plunge	Value	Trend	Plunge
EVT1	188.7	76.4	43.4	55.4	−72.0	42.0	32.9	−177.4	16.4
EVT2	358.6	−130.1	25.0	68.6	77.0	62.4	−84.3	−34.9	11.0
EVT3	2710.0	−133.5	29.0	556.7	56.0	60.6	−483.0	−41.2	4.0
EVT4	372.5	−145.5	3.5	62.4	105.9	79.2	−122.8	−54.9	10.2
EVT5	30.1	−147.9	12.0	3.6	−7.0	74.7	−15.9	120.1	9.4
EVT6	115.7	35.4	27.8	18.3	−135.4	61.9	−42.6	127.4	3.8
EVT7	286.1	52.3	69.8	80.4	−49.3	4.2	35.6	−140.8	19.8
EVT8	891.9	−137.1	20.1	155.9	93.8	59.9	−268.2	−38.8	21.5
EVT9	191.3	40.6	12.1	43.9	171.2	71.8	−15.6	−52.4	13.4
EVT10	2033.0	−121.1	36.0	332.9	88.0	50.3	−701.7	−20.2	14.5
EVT11	103.1	−139.8	39.0	20.4	17.1	48.7	−21.7	120.6	11.6
EVT12	365.5	−117.5	6.6	48.4	−24.5	23.9	−172.1	138.1	65.1
EVT13	356.5	−130.8	34.0	64.3	7.5	47.9	−99.4	123.6	21.7
EVT14	901.6	−140.5	49.9	214.9	43.2	40.1	−42.0	−48.3	1.8
EVT15	4781.0	−122.7	4.3	63.1	120.5	80.5	−4529.0	−32.1	8.4
EVT16	400.4	−141.3	31.7	55.6	48.4	57.9	−177.8	−48.6	4.4
EVT17	69.1	−130.3	13.5	6.3	−21.8	52.9	−44.0	130.5	33.8
EVT18	553.3	−126.1	15.1	35.8	−22.3	41.5	−410.3	128.4	44.6

[a]Eigenvalues are given in 10^{15} N m. Trend and plunge are given in degrees clockwise from north and degrees below horizontal, respectively.

Table 8. FMT Solutions for Miyakejima Earthquakes[a]

	T Axis			I Axis			P Axis		
Event	Value	Trend	Plunge	Value	Trend	Plunge	Value	Trend	Plunge
EVT1	189.9	82.6	54.3	109.1	−98.8	35.7	46.6	−8.3	0.6
EVT2	338.9	−129.5	26.4	135.5	70.0	62.2	−72.8	−35.5	8.0
EVT3	2508.0	−133.1	27.4	98.2	23.3	60.5	−599.7	131.6	10.1
EVT4	373.5	−148.3	5.5	97.6	81.5	81.5	−115.2	−57.7	6.5
EVT5	31.3	−150.1	15.6	3.7	−9.6	70.2	−18.3	116.5	12.0
EVT6	103.6	34.2	23.6	13.9	−139.0	66.3	−47.3	125.3	2.5
EVT7	222.3	41.9	64.2	80.0	−55.8	3.7	17.1	−147.6	25.5
EVT8	880.2	−136.5	21.9	258.4	63.2	66.9	−185.1	−43.6	7.0
EVT9	163.5	37.0	6.8	−25.7	−54.7	14.1	−74.3	152.2	74.3
EVT10	2063.0	−122.1	39.2	665.9	82.8	48.1	−621.9	−21.6	12.6
EVT11	88.7	−141.8	35.1	27.3	15.9	52.8	−24.7	120.5	10.9
EVT12	435.1	−109.5	23.3	63.4	−11.3	18.3	−257.8	113.1	59.6
EVT13	380.1	−128.5	35.3	43.7	−4.3	38.4	−148.3	115.3	32.0
EVT14	845.6	−145.1	50.9	278.6	48.9	38.3	−55.6	−46.6	6.9
EVT15	4951.0	−123.9	7.4	1125.0	102.4	79.4	−4006.0	−32.9	7.6
EVT16	491.6	−142.9	42.6	164.8	43.1	47.2	−144.8	−50.2	3.0
EVT17	80.2	−125.8	23.0	25.1	−7.5	48.1	−43.1	128.3	32.8
EVT18	689.1	−120.8	27.3	208.5	−4.1	41.0	−299.9	126.4	36.8

[a]Eigenvalues are given in 10^{15} N m. Trend and plunge are given in degrees clockwise from north and degrees below horizontal, respectively.

variance reduction but because it can be interpreted in terms of plausible source processes.

[16] Most of the earthquakes studied had nondouble-couple source mechanisms. The locations of these earthquakes, the tensile nature of their mechanisms, and the orientations of those tensile components are all consistent with a northwest striking dike intrusion (Figure 1). The largest nondouble-couple earthquake in the Miyakejima sequence is EVT3, an M_w 6.2 event located on the northwestern tip of the inferred dike intrusion. It has a tensile source mechanism which could indicate that EVT3 was related to inflation or propagation of the offshore dike.

[17] Some of the earthquakes in the Miyakejima sequence are double-couple events. One example of this type of earthquake is EVT15. The seismic data are well fit by a simple solution consisting of a vertical strike-slip mechanism, and EVT15 is located well south of the inferred dike intrusion (Figure 1). This suggests that EVT15 is a tectonic earthquake with fault-parallel slip on a planar rupture, possibly triggered by the nearby dike intrusion [*Toda et al.*, 2002].

[18] One of the most unusual source mechanisms in this study belongs to EVT7. This earthquake was located on Miyakejima at ~1 km depth and occurred during the first summit eruption of Mount Oyama [*Geshi et al.*, 2001]. (The results of the FMT inversion for EVT7 are shown in Figure 7.) The waveforms for this earthquake are complex: the observed Rayleigh waves have nearly constant amplitude and phase, which is a characteristic of isotropic sources, yet there are large amplitudes on the tangential component. The character of the Rayleigh waves for EVT7 is noticeably different than for EVT3 (Figure 5). An explosion mechanism only produces longitudinal waves; so the observed SH radiation indicates that there is an additional nonisotropic component. While the reported moment magnitude of EVT7 was 3.7, the results of our

Table 9. Moment, Moment Magnitude, and Epsilon Values for Nonvolumetric Earthquake Source Models[a]

	DC			Deviatoric		
Event	Moment	M_w	ε	Moment	M_w	ε
EVT1	101.00	5.34	0	77.76	5.26	0.178
EVT2	245.70	5.59	0	230.70	5.58	0.387
EVT3	1775.00	6.17	0	1814.00	6.17	0.377
EVT4	328.80	5.68	0	282.90	5.63	0.439
EVT5	26.29	4.95	0	25.83	4.94	0.264
EVT6	76.99	5.26	0	76.95	5.26	0.335
EVT7	42.44	5.09	0	91.40	5.31	0.365
EVT8	662.60	5.88	0	623.50	5.86	0.400
EVT9	154.30	5.46	0	140.30	5.43	0.227
EVT10	1118.00	6.03	0	1329.00	6.08	0.277
EVT11	58.96	5.18	0	56.83	5.17	0.277
EVT12	324.80	5.67	0	397.30	5.73	0.052
EVT13	263.40	5.61	0	278.00	5.63	0.156
EVT14	341.90	5.69	0	404.30	5.74	0.395
EVT15	4655.00	6.45	0	4395.00	6.43	0.027
EVT16	283.70	5.64	0	298.90	5.65	0.380
EVT17	65.57	5.21	0	66.22	5.21	0.001
EVT18	480.50	5.79	0	546.10	5.82	0.006

[a]Moment is given in 10^{15} N m. Note that for DC mechanisms, $\varepsilon = 0$ by definition.

Table 10. Moment, Moment Magnitude, and Epsilon Values for Nondeviatoric Earthquake Source Models[a]

	DC + ISO			CDC			FMT		
Event	Moment	M_w	ε	Moment	M_w	ε	Moment	M_w	ε
EVT1	139.60	5.43	0	141.00	5.43	0.383	158.30	5.47	0.082
EVT2	251.20	5.60	0	264.90	5.62	0.187	263.10	5.61	0.008
EVT3	1817.00	6.17	0	1986.00	6.20	0.208	1825.00	6.17	0.310
EVT4	283.30	5.63	0	280.80	5.63	0.155	284.90	5.64	0.083
EVT5	25.67	4.94	0	24.22	4.92	0.098	25.75	4.94	0.072
EVT6	91.50	5.31	0	88.11	5.30	0.143	81.13	5.27	0.119
EVT7	113.40	5.37	0	211.60	5.55	0.352	167.50	5.48	0.229
EVT8	699.60	5.90	0	667.70	5.88	0.165	661.70	5.88	0.106
EVT9	154.00	5.46	0	139.30	5.43	0.248	128.30	5.41	0.329
EVT10	1427.00	6.10	0	1539.00	6.12	0.150	1595.00	6.14	0.027
EVT11	82.23	5.28	0	75.85	5.25	0.196	67.93	5.22	0.054
EVT12	286.70	5.64	0	287.70	5.64	0.113	360.40	5.70	0.047
EVT13	249.60	5.60	0	265.60	5.62	0.172	290.20	5.64	0.167
EVT14	589.40	5.85	0	656.10	5.88	0.264	630.80	5.87	0.159
EVT15	4841.00	6.46	0	4657.00	6.45	0.009	4573.00	6.44	0.093
EVT16	359.00	5.70	0	312.30	5.66	0.121	380.70	5.72	0.018
EVT17	63.20	5.20	0	58.09	5.18	0.071	66.77	5.22	0.069
EVT18	495.10	5.80	0	487.70	5.79	0.048	551.40	5.83	0.019

[a]Moment is given in 10^{15} N m. Note that for DC + ISO mechanisms, $\varepsilon = 0$ by definition.

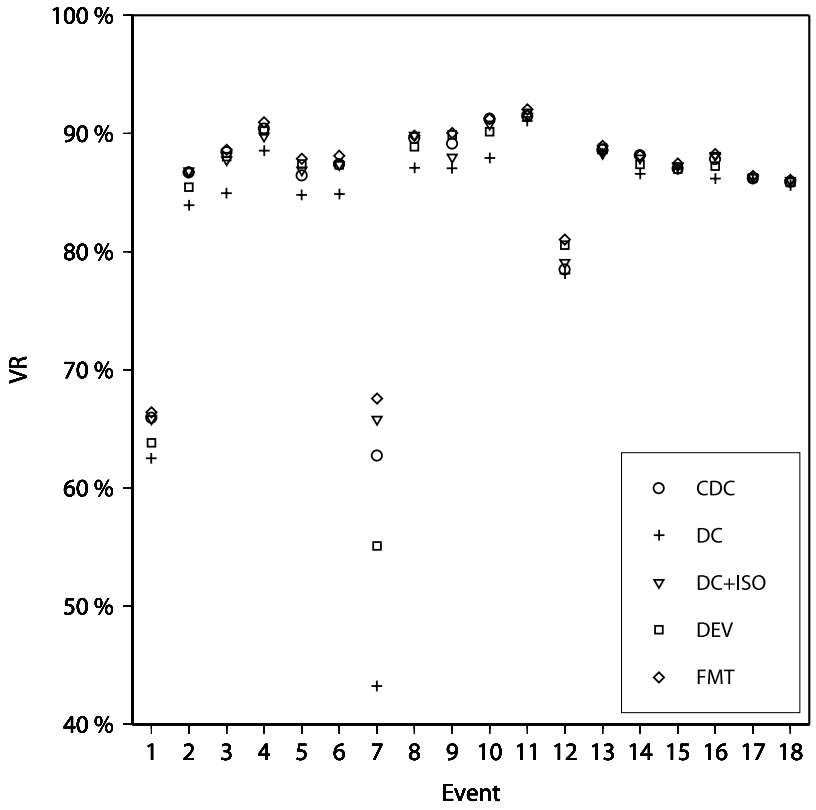

Figure 4. Comparison of variance reduction (VR) values for all five source models and 18 earthquakes.

long period inversion show that it was actually an M_w 5.3 earthquake. The source mechanism is extremely nondouble-couple and contains a large isotropic component. As Figure 4 shows, the CDC mechanism does not fit the data as well as either the DC + ISO or the FMT solution, and the difference in fit between the CDC and the explosive source solutions is the same or more than the difference between the DC mechanism and the more complex mechanisms for the other events. Thus, from the moment tensor analysis, it seems that the volumetric source component of EVT7 is more isotropic than tensile. The explosive characteristic of the source mechanism and the temporal and spatial relationship of the source to the eruption strongly suggest that this earthquake was related to eruption processes. The positive volume change associated with this source could indicate that it is related to magma escape at depth. Gravity studies of the Miyakejima eruption and subsequent caldera collapse indicate that a significant mass of magma drained from the magma chamber, weakening the volcanic edifice and contributing to the caldera collapse [*Furuya et al.*, 2003].

[19] Kikuchi and Yamanaka (EIC note, 2000, http://www.eri.u-tokyo.ac.jp/topics/MIYAKE_E/EIC_Note/000708.html) note that EVT7 was enriched in long period energy. Although the ground shaking was weak, the amplitude of long-period waves was comparable to that of an M5 earthquake. The unusual character of this event prompted Kikuchi and Yamanaka to invert seismograms from three stations in the F-net Broadband Seismograph Network. They inverted the data using two force systems: one is a full moment tensor (6 elements) and the other is a single force. Both models fit the data equally well. The solution with the full moment tensor has a large isotropic component, and is similar to our solution. In the other model (single force), a double-sided single force with a maximum impulse for each side of 2.4×10^{12} Ns was obtained. *Kikuchi et al.* [2001] further investigated this event using two close-in strong motion seismograms recorded on Miyakejima. They obtained a double-sided single force, upward for the first 6 s and downward for the following 6 s, with an impulse of 2.8×10^{12} N s. The vertical single force cannot explain the observed transverse components (Figure 7). Thus the force must have some horizontal component. With the field evidence of a large-scale collapse in the caldera [*Nakada et al.*, 2001], *Kikuchi et al.* [2001] preferred the single-force solution, and interpreted it as a collapse of a cylindrical mass with a diameter of 300 m and a height of 300 m over a vertical distance of 200 m. Considering the field evidence, we believe that, for this event, the single-force model is probably more appropriate than any moment tensor model.

6. Event Kinematics From GPS Data

[20] The two largest earthquakes differ from each other in their settings and mechanisms. EVT15 has a moment magnitude 6.4, and is located south of the inferred dike intrusion. In contrast, the M_w 6.2 EVT3 is located near the tip of the inferred dike intrusion. It has a very nondouble-couple mechanism which appears to be directly related to the dike intrusion. Both of these earthquakes are large enough to generate significant static displacements at several continuous GPS stations operated by the Geographical

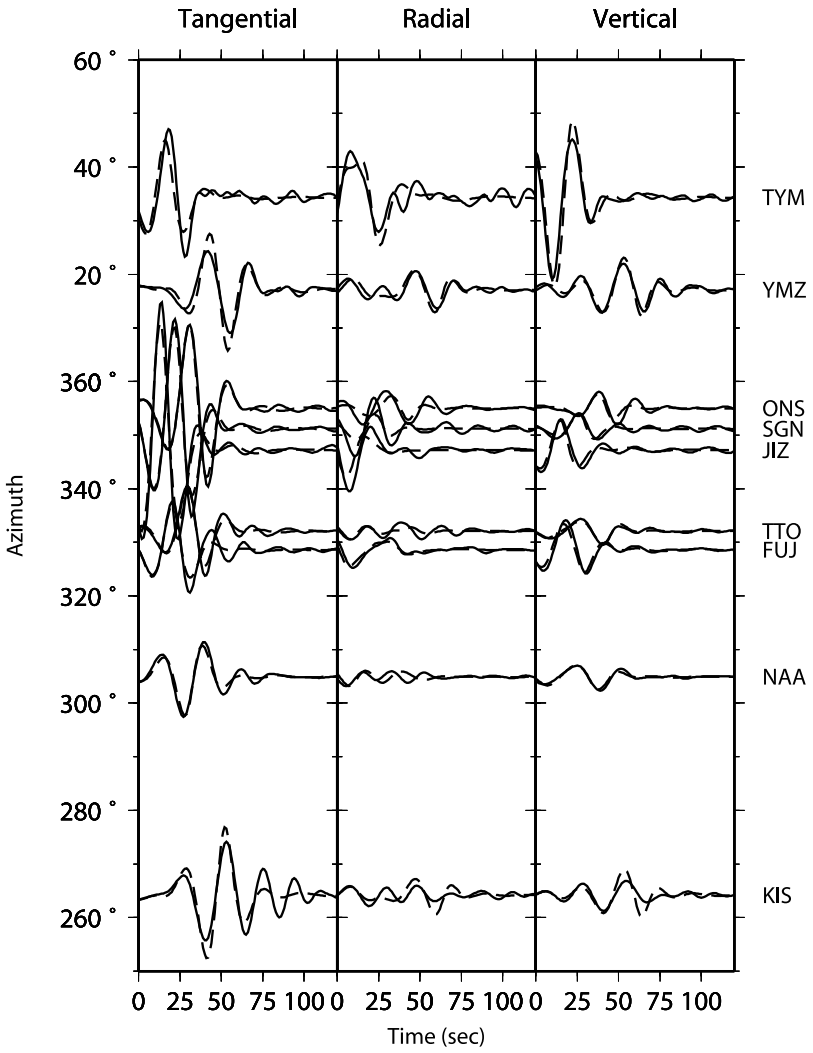

Figure 5. Comparison of EVT3 data (solid line) to synthetics (dashed line) for the CDC moment tensor inversion.

Survey Institute of Japan (GSI) [*Nishimura et al.*, 2001]. We model the surface motions caused by these events using rectangular uniform slip dislocations in an elastic half-space [*Okada*, 1985]. Our nonlinear GPS inversion solves for fault geometry, fault location, and slip components, which minimize the misfit (weighted-residual sum of squares, WRSS) of the model [*Bürgmann et al.*, 1997]. The displacement discontinuity is composed of two slip components parallel to the dislocation plane as well as an opening component perpendicular to the fault. This is kinematically equivalent to the type of source modeled by the CDC moment tensor decomposition.

[21] Using daily 24 hour GPS solutions and assuming that the coseismic displacements are the difference between the station coordinates on the day before and the day after the earthquake, we observe that EVT15 produced a simple displacement pattern that is well fit by a vertical double-couple mechanism, favoring the northerly striking nodal plane that is also indicated by the north-south alignment of aftershocks (Figure 8). The GPS inversion has a WRSS of 392.6 and a reduced WRSS of 8.5 (Tables 11–13). Because the CDC moment tensor is equivalent to the displacement sources of *Okada* [1985], the moment tensor elements can be directly calculated from the geodetically determined slip magnitude and direction (see the appendix). We can then use the geodetic source mechanism and our existing seismic Green's functions for this earthquake to forward predict the seismic data. Using this mechanism to forward predict the observed seismograms, we find that the GPS-derived source fits the seismic data with a variance reduction of 74.3% (Figure 9). So the GPS data are capable of constraining the mechanism of this earthquake and can forward predict the seismic data, a completely independent data set. We also considered GPS models which included opening as well as double-couple slip. By including this additional free parameter in the GPS inversion, we were able to reduce the WRSS to 294.0 (reduced WRSS 6.5). However, this model was not consistent with the seismic mechanism for EVT15. Synthetic seismograms computed from a model with opening fit the seismic data with a variance reduction of just 48.2%.

[22] Because of large displacements on Miyakejima on the day of EVT3 (Figure 10) that are related to the local caldera deflation and not EVT3, we were not able to use

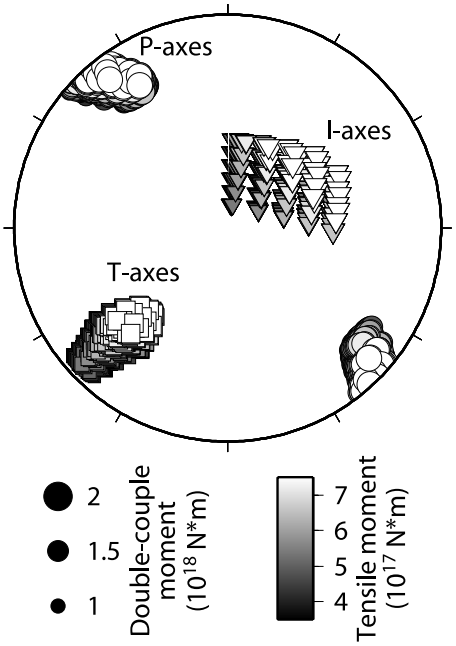

Figure 6. Empirical uncertainty bounds on the CDC mechanism for EVT3. The principle axes of all CDC mechanisms which fit the data with a decrease of 5% or less in variance reduction from the best fit mechanism are plotted in lower hemisphere equal-area projection. Maximum tension directions (T axes) are denoted by squares, maximum compression directions (P axes) are denoted by circles, and the directions of the eigenvectors corresponding to intermediate eigenvalues (I axes) are denoted by triangles. Symbols are scaled according to the moment of each mechanism's double-couple component and colored according to the tensile moment. The scatter of axis orientations and moments is small, showing that the CDC mechanism for EVT3 is quite stable. Also, since no mechanism with zero tensile moment fits the data sufficiently well, a nondouble couple is a required part of the CDC solution for this earthquake.

daily GPS solutions. Instead, we calculated 30 s epoch solutions using GIPSY software [*Lichten and Border*, 1987]. The orbits of the GPS satellites are constrained to agree with the IGS precise ephemerides [*Beutler et al.*, 1994] and Earth orientation. The position of one station, Usuda (USUD), is tightly constrained to its ITRF2000 position [*Altamimi et al.*, 2002] and the positions of the other sites are estimated relative to it. Other estimated parameters include satellite and receiver clocks, zenith atmospheric delay parameters and carrier phase biases. GIPSY provides various noise models for positioning estimates. We used a random walk parameterization similar to that described by *Larson et al.* [2002] that produces smoother time series than would be evident if the positions were assumed to be independent. The main difference here is that we allowed the position at each site to change without constraint at the origin time of EVT3. However, the short epoch processing cannot well constrain the vertical component of the deformation field, and so we weight our inversion to fit only the horizontal displacements. Also, we assume an uncertainty of 5 mm on each horizontal component of displacement for the 30 s epoch solutions as opposed to the typically 3 mm uncertainties for the daily solutions. We find that the offsets at the three stations closest to the EVT3 hypocenter, which should at most be only slightly affected by the Miyakejima deflation, are nearly identical in the daily solution and the 30 s epoch solution.

[23] There are few GPS stations near the EVT3 hypocenter which can help us constrain the source mechanism. Thus we can satisfy the geodetic data with either a double-couple or a nondouble-couple source. However, we generally prefer the nondouble-couple solution because the seismic data require a nondouble-couple component, and the nondouble-couple geodetic mechanism is more consistent with the aftershock distribution.

[24] Our nondouble-couple GPS inversion yields a model that fits the motions at the GPS stations nearest the EVT3 hypocenter (Figure 11). The fault orientation and slip in this model are compatible with the seismic source mechanism. The strike-slip, dip-slip, and tensile displacements are 0.5042 m, 0.1893 m, and 0.1752 m, respectively. This model fits the GPS data with a WRSS of 73.9 (reduced WRSS 2.7). Notably, the GPS inversion produces a model with a fault that ends at the locations where EVT3 aftershocks are clustered.

[25] The main discrepancy with the seismic mechanism is that the moment of the GPS model is 4.2 times larger than the seismic moment for EVT3. This means that most of the displacement related to this nondouble-couple tensile event was not seen seismically. In order to predict the observed seismograms, we had to scale down the moment of the GPS mechanism. This produces a model which fits the seismic data with a variance reduction of 73.5% (Figure 12). Thus the GPS mechanism is geometrically consistent with the seismic mechanism, and independently points to the same source processes.

7. Discussion

[26] We have applied a kinematically realistic moment tensor decomposition (CDC) to earthquakes from the 2000 Miyakejima eruption sequence to model both seismic waveforms and GPS observations of surface offsets. Although we have not included any joint seismic and geodetic inversions in this study, the CDC model could be used for joint modeling as well as separate seismic and geodetic inversions. Other moment tensor models fit the seismic data well, but we prefer the CDC model because while the deviatoric and DC + ISO mechanisms have the same number of free parameters as the CDC model, there is no obvious way to interpret them in terms of realistic mechanical source processes. The CDC model is based on a simple kinematic source model of a fault plane with both in-plane and tensile slip components.

[27] Most of the studied earthquakes have mechanisms which appear to be related to the inflation of the dike (Figure 1). Inversions of GPS data show that EVT3 is related to the dike intrusion while EVT15 is a strike-slip earthquake that does not appear to be volcanic in nature. The GPS mechanism for EVT15 is very similar to the seismic mechanism and successfully forward predicts the

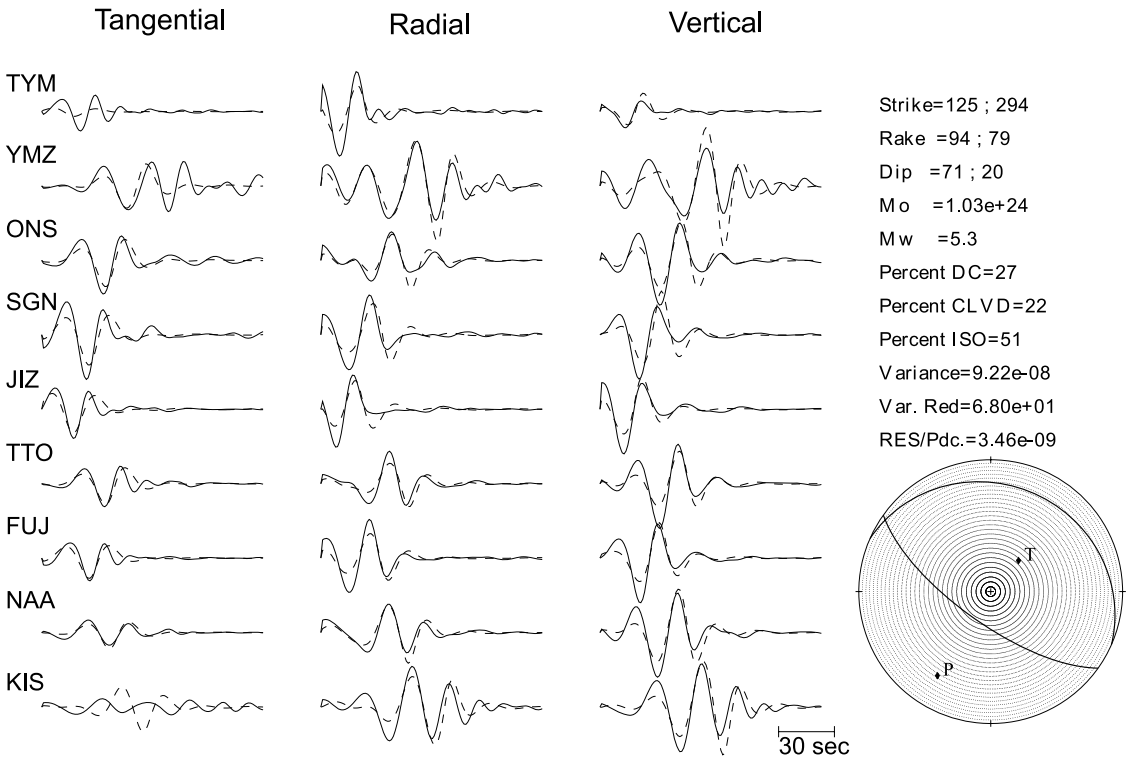

Figure 7. Results of FMT inversion for EVT7. Note the very large isotropic component.

observed seismograms. The kinematic parameters we obtained for the event are consistent with those derived by *Nishimura et al.* [2001] (Tables 11–13). The GPS mechanism for EVT3 is similar in geometry to the CDC seismic mechanism, but it has a significantly larger moment than the seismic mechanism.

[28] The discrepancy between the geodetic and seismic moments for EVT3 is very interesting. If the geodetic moment is to be believed, then EVT3 was as large as the largest earthquake in the Miyakejima sequence, EVT15. It is possible that the EVT3 source process had a very slow deformation component which was outside of the frequency passband used in our seismic moment tensor inversions but was captured by the GPS data, and that it was the contribution from the slow source process which greatly increased the geodetic moment.

[29] For GEONET GPS receivers, the typical period of errors due to multipath effects and poor constellation geometry is 100 to 200 s, which is too short to removed from 30 s positioning time series using traditional high-frequency GPS methods such as those of *Choi et al.* [2004] or *Larson et al.* [2007]. Instead, we use a random walk parameterization similar to that described by *Larson et al.* [2002] for detecting the motion of ice sheets in Greenland. This method uses a Kalman filter which produces a smoother time series than if the positions were assumed to be independent. The difference in this study is that we allowed the position at each site to change without constraint at the origin time of EVT3. However, by enforcing smoothness before and after the origin time, we lose our ability to detect short-term variations (30 s to 5 min) that might be real geophysical signals. It also means that our

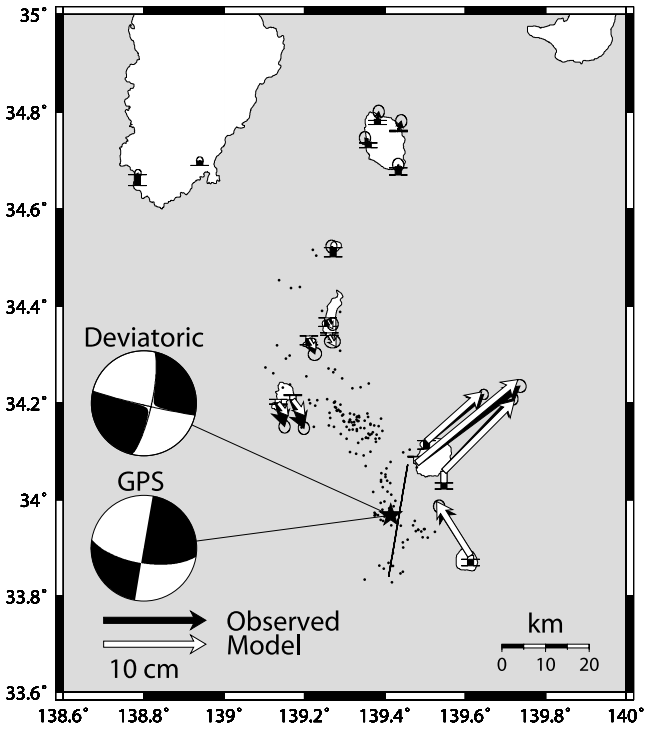

Figure 8. Results of inverting GPS data for EVT15. The GPS mechanism has a strike, dip, and rake of 190°, 90°, and 24°, respectively, and a moment of 6.3×10^{18} N m. This mechanism fits the GPS data with a WRSS of 392.6 and a reduced WRSS of 8.5. The GPS mechanism is very similar to the seismic mechanism, and the deviatoric mechanism for EVT15 is plotted for comparison.

Table 11. Fault Orientations for EVT15 and EVT3 Determined From GPS Data[a]

Event	Latitude	Longitude	Length, km	Width, km	Depth, km	Strike	Dip	Rake
EVT15 shear	33.8401°	139.4093°	26.3	6.5	1.0	190°	90°	24°
EVT15 complete	33.8353°	139.4099°	26.9	6.6	0.9	189°	90°	26°
EVT15 [*Nishimura et al.*, 2001]	33.872°	139.386°	20.0	10.0	2.3	11°	85°	347°
EVT3 shear	34.2161°	139.0851°	14.2	25.0	0.2	288°	60°	220°
EVT3 complete	34.2266°	139.1281°	14.3	25.0	1.9	294°	71°	201°
EVT3 [*Nishimura et al.*, 2001]	34.210°	139.208°	15.8	7.9	0.1	100°	41°	204°

[a]The latitude and longitude of the western edge of the faults are given. Results are given for shear-slip only models (shear) as well as models which allow for both shear and opening (complete). For comparison, we include the inversions from *Nishimura et al.* [2001] in which the length, width, strike, dip, and rake are fixed.

GPS displacements are sensitive to much longer period deformation than our seismic moment tensor inversions which use data filtered between 20 and 50 s.

[30] To test whether there are both fast and slow deformation components to EVT3, we compare velocity waveforms and Fourier amplitude spectra for both EVT3 and EVT15 (Figure 13). Recall that EVT15 has a simple double-couple mechanism, and its moment (Mw 6.4) is the same for both the geodetic and seismic waveform data. Our moment tensor inversions for EVT3, which use seismic data filtered between 20 and 50 s, indicate that EVT3 was a smaller Mw 6.2 earthquake. Figure 13 shows that at frequencies within the range used in our moment tensor inversions, the velocity amplitudes at station SGN are significantly larger for EVT15 than EVT3. However, at the longest periods, EVT3 increases in amplitude becoming comparable to EVT15. This indicates that there is a very long period component to the EVT3 source process. Figure 13 suggests that EVT3 and EVT15 become comparable only at periods longer than 200 s, which is much longer than the 50 s corner frequency used for filtering the seismic data, but is compatible with the frequency content of the GPS displacements.

[31] It appears that EVT3 contains two separate source components. One is a fairly fast, very nondouble-couple component, and this is the component to which the seismic moment tensor is most sensitive. The other is a much slower component which dominates at periods of 200 s or greater, and which is detected in the GPS displacements. The slow component produced significant moment, causing the total geodetic moment to be approximately 4 times as large as the seismic moment. Since the geodetic mechanism is more double-couple than the seismic mechanism, this long period source process may consist mainly of shear slip.

[32] *Nishimura et al.* [2001] relied on 6 hour GPS solutions to obtain a model of EVT3 that does not allow for an opening component. They assume an oblique-slip mechanism and invert for slip to determine a geodetic moment of 5.39×10^{18} N m. Although the *Nishimura et al.* [2001] model is based on a priori assumptions of fault geometry and slip direction that are different from the optimal values we obtained by inverting for those parameters, this value is comparable with the moment of the DC component of our geodetically determined source mechanism for EVT3. It also supports our finding that there is a large amount of slow slip associated with EVT3.

[33] We can calculate the net volume change of the earthquake sources from the isotropic moments for these events. Using the results of the CDC moment tensor inversions, we find that the total volume change associated with these 18 earthquakes is 0.035 km^3 (Table 14), which is only 4% of the total 0.94 km^3 volume increase associated with the dike intrusion [*Furuya et al.*, 2003]. This indicates that most of the volumetric changes accompanying the dike intrusion were not accommodated by large earthquakes.

8. Conclusions

[34] Using regional broadband seismic data, we have determined source mechanisms for 18 earthquakes which occurred as part of the Miyakejima eruption and dike intrusion in 2000. Many of these earthquakes have non-double-couple mechanisms related to the inflation and propagation of an offshore dike. We have estimated moment tensor solutions using several common moment tensor models (deviatoric, DC + ISO and full moment tensor) as well as the "crack + double-couple" model (CDC). Although all of these models fit the data almost equally well, we argue for the CDC model because it is both a plausible

Table 12. Displacements, Moments, and Weighted-residual Sum of Squares for the GPS Models in Table 10[a]

Event	Strike Slip, m	Dip Slip, m	Opening, m	DC Moment, N m	Tensile Moment, N m	WRSS	Reduced WRSS
EVT15 shear	1.1234 ± 0.0098	0.4928 ± 0.0148	—	6.30×10^{18}	—	392.6	8.5
EVT15 complete	1.0992 ± 0.0108	0.5405 ± 0.0195	0.0281 ± 0.0068	6.58×10^{18}	0.15×10^{18}	378.0	8.4
EVT15 [*Nishimura et al.*, 2001]	1.08	0.25	—	6.66×10^{18}	—	—	—
EVT3 shear	0.4569 ± 0.0360	0.3841 ± 0.0438	—	6.37×10^{18}	—	75.4	2.7
EVT3 complete	0.5042 ± 0.0638	0.1893 ± 0.0511	0.1752±0.0182	5.77×10^{18}	1.88×10^{18}	73.9	2.7
EVT3 [*Nishimura et al.*, 2001]	1.31	0.59	—	5.39×10^{18}	—	—	—

[a]WRSS, weighted-residual sum of squares. Moments are calculated assuming $M_0 = \mu AD$ where $\mu = 3 \times 10^{10}$ Pa, A is the area of the fault (Table 11), and D is the magnitude of the slip vector which is not parallel to the fault plane for EVT3. The reduced WRSS values are given by WRSS/(N-P) where N is the number of observations and P is the number of free parameters in the model.

Table 13. Bounds Used to Constrain Geodetic Inversions Reported in This Paper

	Length, km	Width, km	Depth, km	Dip	Strike	Center Latitude	Center Longitude
			EVT15				
Min	12.7	6.5	0	70°	180°	33.92°	139.30°
Max	38.0	18.6	30	90°	208°	34.05°	139.50°
			EVT3				
Min	1.0	0.1	0	60°	256°	34.10°	139.10°
Max	25.0	25	10	79°	300°	34.20°	139.40°

model for earthquake source processes in volcanic regions and because it can be used to fit geodetic data as well as seismic data. This latter feature of the CDC model allows us to use the source mechanisms determined with geodetic data to forward predict observed seismograms. We find for the two largest earthquakes in the sequence, EVT3 and EVT15, that the geodetic mechanisms generally agree with the seismic data. However, the geodetic moment for EVT3 is significantly larger than the moment determined from inverting the seismic data. We conclude that there was a long, slow (greater than 200 s period) double-couple slip component to the EVT3 source process in addition to a fast, largely tensile component.

Appendix A: Derivation and Interpretation of CDC Moment Tensor Decomposition

A1. Derivation of the CDC Model

[35] Because seismic moment tensors must be symmetric, any moment tensor can be described by six independent elements. There is no unique way to decompose moment tensors. However, in this study, we argue for the use of a moment tensor decomposition [*Dufumier and Rivera*, 1997] which is physically realistic and suitable for moment tensor inversions. We propose to describe a seismic source as the sum of one shear dislocation and one tensile dislocation where the direction of opening is perpendicular to the fault

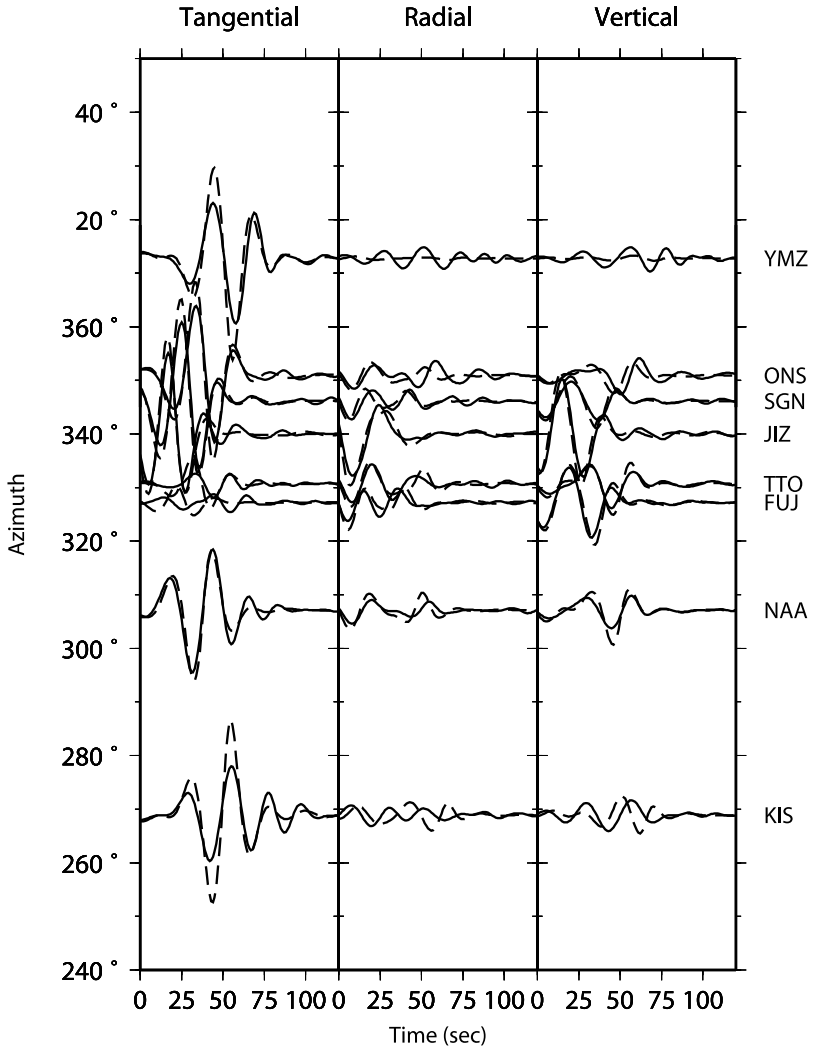

Figure 9. Comparison of EVT15 data (solid line) to synthetic seismograms generated from the GPS mechanism (dashed line). The mechanism determined from GPS data accurately predicts the seismic data, which are a completely independent data set, with a VR of 74.3%.

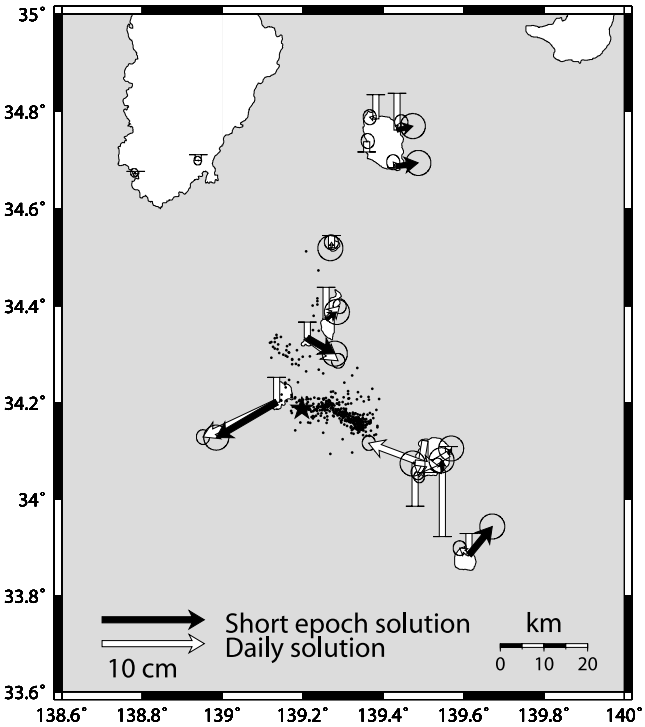

Figure 10. Comparison of 24 hour epoch and 30 s epoch GPS solutions for EVT3 coseismic deformation. The daily solution contains a large amount of subsidence on Miyakejima which is probably related to deflation of the magma chamber beneath Mount Oyama. This aseismic volcanic deformation masks much of the coseismic signal from EVT3. Thus we found it necessary to employ short epoch solutions in our EVT3 GPS source mechanism inversions.

plane of the double-couple (Figure 2). Thus the crack wall and the double-couple's fault plane are coincident and have the same orientation given by the same strike and dip. This model, which we will refer to as CDC for crack + double-couple, is consistent with processes which we might expect to observe in volcanic settings.

[36] The CDC model consists of the summation of a double-couple source and a tensile crack source. Let us consider a fault plane with area S, slip D, in a homogeneous medium with Lamé's parameters λ and μ. We define the double-couple and opening moments as $M_0 = \mu S D_{\|}$ and $M_C = \lambda S D_{\perp}$, respectively, where $D_{\|}$ and $D_{\perp}$ are the fault parallel and normal slip components of the slip vector, respectively.

[37] *Aki and Richards* [2002] show that the moment tensors for a double-couple (DC) and tensile source are given by

$$\mathbf{M}^{\mathbf{DC}} = \begin{bmatrix} 0 & 0 & 0 \\ 0 & -M_0 & 0 \\ 0 & 0 & M_0 \end{bmatrix} \tag{A1}$$

$$\mathbf{M}^{\mathbf{tensile}} = \begin{bmatrix} M_C & 0 & 0 \\ 0 & M_C & 0 \\ 0 & 0 & \left(\frac{1}{\nu} - 1\right) M_C \end{bmatrix} \tag{A2}$$

where ν is the Poisson ratio of the medium, and we adopt the northeast-down coordinate system of *Aki and Richards* [2002].

[38] Before we can sum these two tensors to produce the CDC model, we must first project the double-couple tensor into the reference frame of the principal coordinates of the tensile component. The eigenvector of the double-couple component associated with the intermediate eigenvalue (the null axis) lies in the fault plane. The other two eigenvectors (the T axis and P axis), are oriented at an angle of 45° to the fault plane. The major dipole of the tensile component is normal to the wall of the crack, while the two minor dipoles lie in the plane of the crack. Since we require that the wall of the crack be coincident with the fault plane, we obtain the desired transformation by rotating the double-couple component ±45° about the null axis. In the principal coordinates of the tensile component, the moment tensor of the double couple is

$$\mathbf{M}^{\mathbf{DC}} = \begin{bmatrix} 0 & 0 & 0 \\ 0 & 0 & \pm M_0 \\ 0 & \pm M_0 & 0 \end{bmatrix} \tag{A3}$$

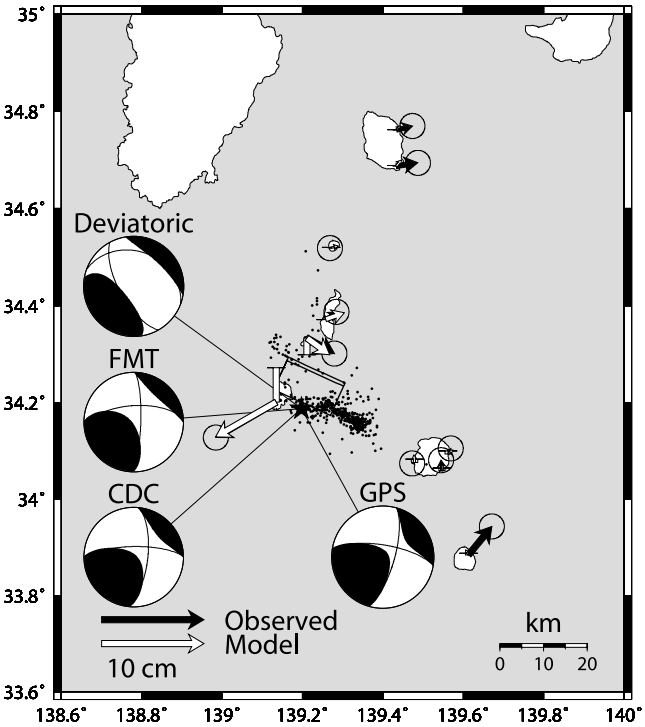

Figure 11. Same as Figure 8 for EVT3. Because of the complex Miyakejima deflation pattern present in the daily solution, we used short epoch (30 s) solutions for our inversion. The GPS mechanism for EVT3 is similar to the mechanisms determined from seismic data. (Note that only the deviatoric part of the seismic and GPS mechanisms are plotted.) The nondouble-couple GPS mechanism has a strike, dip, and rake of 294°, 71°, and 201°, respectively. The moments of the double-couple and tensile components are 5.77×10^{18} and 1.88×10^{18} N m, respectively. The mechanism fits the GPS data with a WRSS of 73.9 and a reduced WRSS of 2.7.

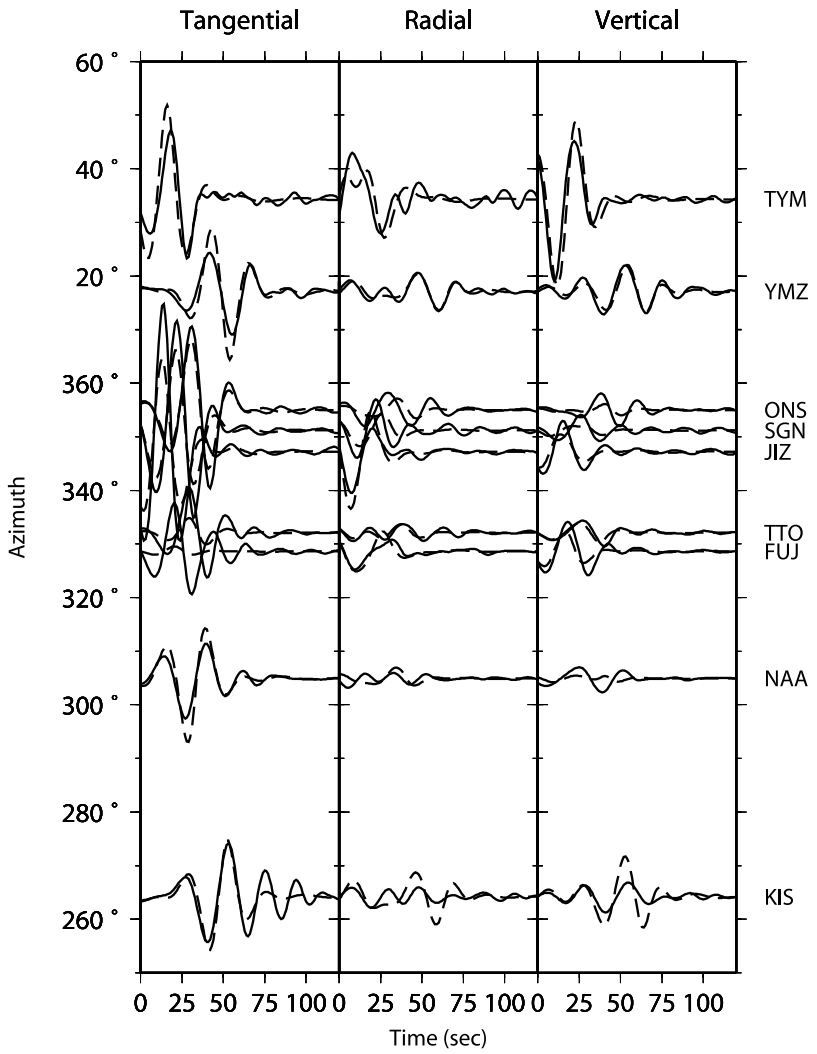

Figure 12. Same as Figure 9 for EVT3. Although the GPS mechanism is very similar to the CDC mechanism, the moment of the GPS mechanism is approximately 4 times larger. This indicates that most of the GPS deformation occurs at periods longer than those used in the seismic moment tensor inversion. The synthetic plotted here has been scaled down to match the seismic moment. The VR of the scaled synthetic is 73.5%.

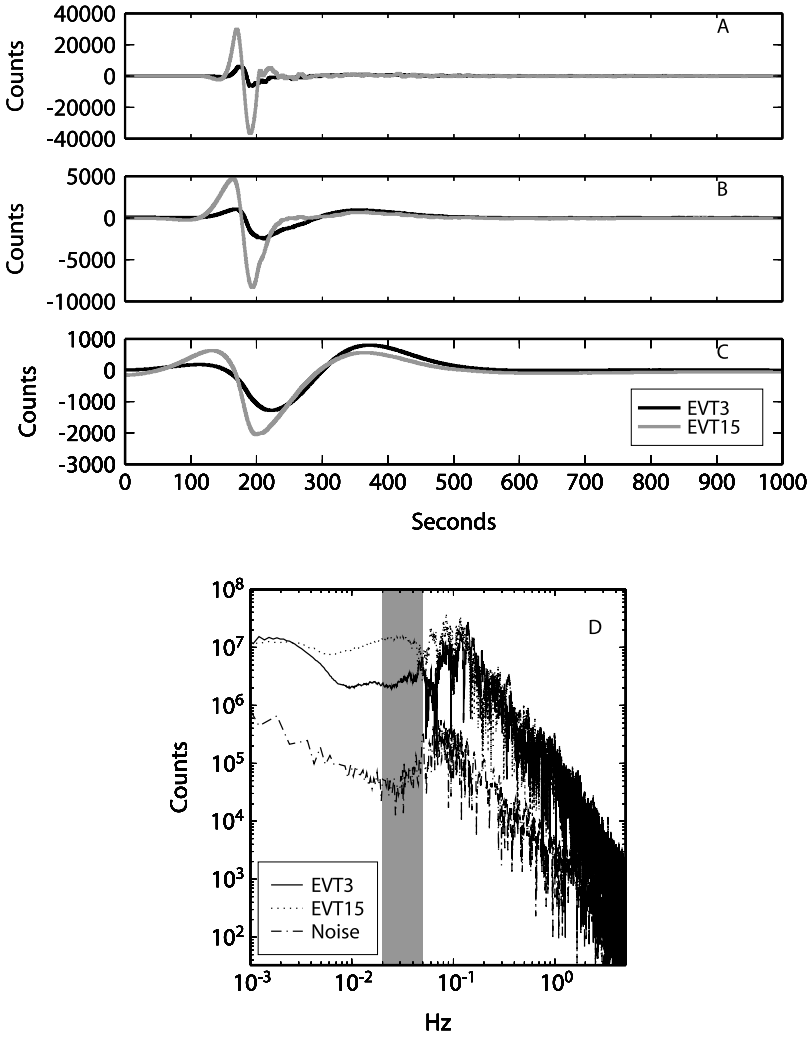

Figure 13. Observed seismograms and spectra for EVT3 and EVT15. The observed velocity seismograms for EVT3 and EVT15 from station SGN are compared in Figures 13a–13c. The seismograms were low-pass filtered with corner frequencies of (a) 0.02 Hz, (b) 0.01 Hz, and (c) 0.005 Hz. (d) Raw broadband spectra for EVT3 and EVT15 are compared to sample spectrum of preevent noise. While EVT15 is clearly a larger earthquake than EVT3 within the frequency range used in our seismic moment tensor inversions (indicated by the shaded region), EVT3 gains in amplitude at lower frequencies becoming slightly larger than EVT15 at the longest periods. This indicates that there is a very slow component of deformation in EVT3 which results in a larger GPS moment than seismic moment.

If we add the two components together (equations (A2) and (A3)) and solve for the eigenvalues of the resulting tensor, we find

$$\mathbf{M}^{\mathbf{CDC}} = \mathbf{M}^{\mathbf{DC}} + \mathbf{M}^{\mathbf{tensile}} = \begin{bmatrix} \frac{M_C}{2\nu} - \beta & 0 & 0 \\ 0 & M_C & 0 \\ 0 & 0 & \frac{M_C}{2\nu} + \beta \end{bmatrix} = \begin{bmatrix} m_3 & & \\ & m_2 & \\ & & m_1 \end{bmatrix} \tag{A4}$$

where

$$\beta = \sqrt{\left(\frac{1-2\nu}{2\nu}\right)^2 M_C^2 + M_0^2} \tag{A5}$$

Note that in all cases, $m_1 \geq m_2 \geq m_3$. In our inversions, we assume a Poisson solid ($\nu = 0.25$), which reduces equations (A4) and (A5) to,

$$\mathbf{M}^{\mathbf{CDC}} = \mathbf{M}^{\mathbf{DC}} + M^{\mathbf{tensile}} = \begin{bmatrix} 2M_C - \beta & 0 & 0 \\ 0 & M_C & 0 \\ 0 & 0 & \end{bmatrix} \tag{A6}$$

and

$$\beta = \sqrt{M_C^2 + M_0^2} \tag{A7}$$

Table 14. Isotropic Moment and Volume Change for CDC Mechanisms[a]

Event	Moment, 10^{15} N m	Volume Change, 10^6 m^3
EVT1	92.325	1.026
EVT2	114.266	1.270
EVT3	927.85	10.309
EVT4	104.04	1.156
EVT5	5.942	0.066
EVT6	30.447	0.338
EVT7	134.03	1.489
EVT8	259.859	2.887
EVT9	73.213	0.813
EVT10	554.835	6.165
EVT11	33.91	0.377
EVT12	80.579	0.895
EVT13	107.134	1.190
EVT14	358.17	3.980
EVT15	105.19	1.169
EVT16	92.712	1.030
EVT17	10.456	0.116
EVT18	59.594	0.662
Total	3144.55	34.939

[a]Volume changes are calculated using the relationship $M_0\ (\infty) = (\lambda + 2\mu)\delta V$ for $\lambda = \mu = 3 \times 1010$ Pa [*Aki and Richards*, 2002].

Dufumier and Rivera [1997] express the moment tensor in (A4) as

$$SD\begin{bmatrix} \lambda\cos\alpha + \mu(\cos\alpha - 1) & 0 & 0 \\ 0 & \lambda\cos\alpha & 0 \\ 0 & 0 & \lambda\cos\alpha + \mu(\cos\alpha + 1) \end{bmatrix} \tag{A8}$$

α is the angle of the slip vector from the fault normal. We see that this is identical to equation (A4) with the definition $\cos\alpha = D_\perp/D$.

[39] It can also be shown that the CDC model (equation (A4), or equivalently equation (A8)) is identical to the general moment tensor for a displacement discontinuity across a surface in an isotropic body [*Aki and Richards*, 2002, equation 3.21].

[40] While the moment tensor constraint for a deviatoric (zero trace) moment tensor is linear and easy to apply, the DC + ISO and CDC constraints are nonlinear. *Dufumier and Rivera* [1997] describe a two-step projection approach to solve the problem, and *Templeton and Dreger* [2006] employ a grid search to find DC + ISO solutions. Similarly, the most straightforward way to solve the CDC inverse problem is by a direct grid search.

A2. Characteristics of the CDC Decomposition

[41] Inspection of equation (A4) or equation (A6) shows that for any given value of ν, the CDC decomposition results in unique values for M_0 and M_C. However, $\mathbf{M}^{\mathbf{DC}}$ was rotated into the principal coordinates of the tensile crack component, and there is an ambiguity in the direction of this rotation. Because of this, there are two possible sets of faulting parameters (strike, dip, and rake) which are consistent with a given CDC moment tensor. This is similar to the characteristics of double-couple moment tensors in that a double-couple moment tensor has a specific scalar seismic moment, but there are two sets of faulting parameters which produce a given double-couple moment tensor. These two sets of fault parameters correspond to two orthogonal fault planes. However, in the CDC model, the angle between these two fault planes is given by

$$\theta = \cos^{-1}\left[\frac{\left(\frac{1-2\nu}{2\nu}M_C + \beta\right)^2 - M_0^2}{\left(\frac{1-2\nu}{2\nu}M_C + \beta\right)^2 + M_0^2}\right] \tag{A9}$$

For a pure double couple, the angle between the two fault planes is 90°, and for a tensile crack, the angle is 0° (Figure A1).

[42] It also should be noted that the two sets of faulting parameters derived from the CDC moment tensor decomposition are not the conjugate fault planes of the same double-couple mechanism. They actually correspond to different double-couple mechanisms. In the limit that the CDC mechanism is completely double couple, the two sets of faulting parameters will be the conjugate fault planes of the same double-couple mechanism.

A3. Calculation of Faulting Parameters From CDC Moment Tensors

[43] The procedure for finding the faulting parameters strike, dip, rake, M_0 and M_C of a CDC is somewhat involved. However, we will briefly outline it. Inspection of equations (A4) and (A6) show that M_0 and M_C may be directly determined from a diagonalized CDC moment tensor since M_C is by definition the intermediate eigenvalue.

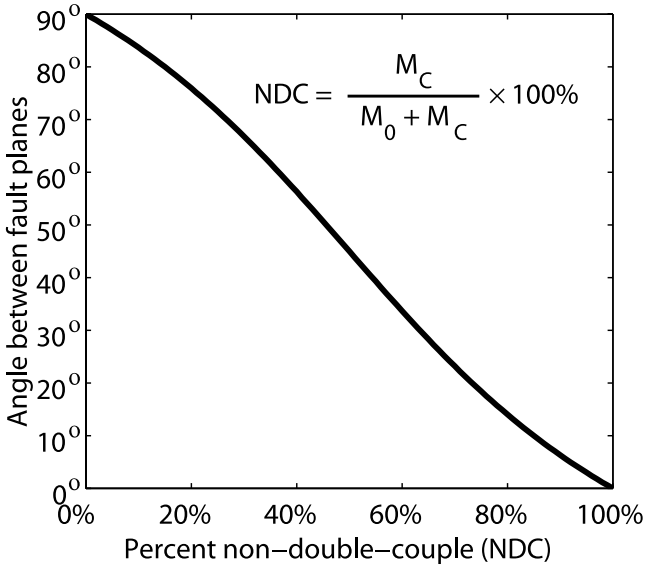

Figure A1. Plot of the angle between the two possible fault plane solutions for a CDC mechanism as a function of increasing tensile component. For zero tensile moment, the mechanism is double couple, and thus the angle between the two fault planes is 90°. Tensile moment tensors are not ambiguous: there is only one fault plane orientation which can produce a given tensile moment tensor. So as the relative strength of the tensile component increases, the angle between the two solutions decreases until it becomes 0° for a completely tensile source.

If the diagonalized CDC moment tensor (equation (A4)) has eigenvectors $\mathbf{v_1}$, $\mathbf{v_2}$, and $\mathbf{v_3}$, associated with eigenvalues m_1, m_2, and m_3, respectively, then the fault normal is given by

$$\hat{\mathbf{n}} = \frac{\left|\frac{1-2\nu}{2\nu}M_C + \beta\right|\mathbf{v_1} \pm \mathbf{v_3}}{\left\|\left|\frac{1-2\nu}{2\nu}M_C + \beta\right|\mathbf{v_1} \pm \mathbf{v_3}\right\|} \quad \text{(A10)}$$

Note that there are two solutions to equation (A10) because CDC moment tensors can be decomposed into two separate fault solutions as discussed in section A2. Once the fault normal is known, we can use it to determine the strike ϕ and dip δ of the fault plane. We can then analytically calculate the moment tensor of the tensile component in Cartesian coordinates,

$$\mathbf{M^{tensile}} = \begin{bmatrix} M_{xx} & M_{xy} & M_{xz} \\ M_{xy} & M_{yy} & M_{yz} \\ M_{xz} & M_{yz} & M_{zz} \end{bmatrix}$$

$$M_{xx} = \sin^2\phi\cos^2\delta \cdot M_C + \cos^2\phi \cdot M_c + \sin^2\delta\sin^2\phi \cdot \left(\frac{1}{\nu} - 1\right)M_C$$

$$M_{xy} = -\sin\phi\cos^2\delta\cos\phi \cdot M_C + \cos\phi\sin \cdot M_C - \sin\delta\sin\phi\cos\phi \cdot \left(\frac{1}{\nu} - 1\right)M_C$$

$$M_{yy} = \cos^2\delta\cos^2\phi \cdot M_C + \sin^2\delta\cos^2\phi \cdot \left(\frac{1}{\nu} - 1\right)M_C$$

$$M_{xz} = -\sin\phi\cos\delta\sin\delta \cdot M_C + \sin\delta\sin\phi\cos\delta \cdot \left(\frac{1}{\nu} - 1\right)M_C$$

$$M_{yz} = \cos\delta\cos\phi\sin\delta \cdot M_C - \sin\delta\cos\phi\cos\delta \cdot \left(\frac{1}{\nu} - 1\right)M_C$$

$$M_{zz} = \sin^2\delta \cdot M_C + \cos^2\delta \cdot \left(\frac{1}{\nu} - 1\right)M_C \quad \text{(A11)}$$

For a Poisson medium, equation (A11) simplifies to

$$M_{xx} = \left[-2\cos^2\delta + 2\cos^2\delta\cos^2\phi - 2\cos^2\phi + 3\right]M_C$$
$$M_{xy} = \left[2\sin\phi\cos^2\delta\cos\phi - 2\cos\phi\sin\phi\right]M_C$$
$$M_{yy} = \left[-2\cos^2\delta\cos^2\phi + 2\cos^2\phi + 1\right]M_C$$
$$M_{xz} = \left[2\sin\phi\cos\delta\sin\delta\right]M_C$$
$$M_{yz} = \left[-2\cos\delta\cos\phi\sin\delta\right]M_C$$
$$M_{zz} = \left[2\cos^2\delta + 1\right]M_C \quad \text{(A12)}$$

A4. Decomposition of a CDC Moment Tensor

[44] The recommended system for decomposing CDC moment tensors is as follows. For each fault plane with normal given by a solution to equation (A10): calculate the strike and dip of that fault plane, use equation (A11) or (A12) to analytically calculate the tensile component for that fault plane, subtract the resulting tensile moment tensor to get the moment tensor of the double-couple component for that fault plane, and finally calculate the rake of the double-couple component consistent with the strike and dip derived from equation (A10). However, care must be taken in calculating the rake at this step. Only the rake of the double-couple mechanism with the fault normal from equation (A10) is a valid solution.

A5. Example CDC Moment Tensor Decomposition

[45] Consider the following moment tensor,

$$\mathbf{M} = \begin{bmatrix} 3 & 1 & 0 \\ 1 & 1 & 0 \\ 0 & 0 & 1 \end{bmatrix} \quad \text{(A13)}$$

$\mathbf{M}$ is composed of a vertical crack with opening in the $\hat{x}$ direction, and a left-lateral vertical strike-slip fault striking in the $\hat{y}$ direction. Thus this is a CDC moment tensor representing coplanar shear and tensile faulting.

[46] The eigenvalues of $\mathbf{M}$ are 3.41, 1.00 and 0.59. Also, by definition of the CDC decomposition, the moment of the crack is equal to the intermediate eigenvalue (M_C = 1.00). Application of equation (A6) for the minimum and maximum eigenvalues results in β = 1.41, and subsequently M_0 = 1.00.

[47] The two possible orientations of the normal to the fault plane ($\hat{n}$) are $n_1 = \langle 1, 0, 0\rangle$ and. $n_2 = \langle 0.707, 0.707,\rangle$. The former case is clearly the prescribed orientation of the above CDC moment tensor. The latter is rotated from the former by 45°.

[48] Considering the n_1 case, the tensile crack moment tensor from equation (A12) is

$$\mathbf{M^{tensile}} = \begin{bmatrix} 3 & 0 & 0 \\ 0 & 1 & 0 \\ 0 & 0 & 1 \end{bmatrix} \quad \text{(A14)}$$

Also, the double-couple moment tensor is

$$\mathbf{M^{DC}} = \mathbf{M^{CDC}} - \mathbf{M^{tensile}} = \begin{bmatrix} 0 & 1 & 0 \\ 1 & 0 & 0 \\ 0 & 0 & 0 \end{bmatrix} \quad \text{(A15)}$$

Equation (A15) is the moment tensor for an east striking, vertically dipping left-lateral mechanism.

[49] For the n_2 case, the tensile crack moment tensor is

$$\mathbf{M^{tensile}} = \begin{bmatrix} 2 & 1 & 0 \\ 1 & 2 & 0 \\ 0 & 0 & 1 \end{bmatrix} \quad \text{(A16)}$$

[50] This moment tensor describes a vertical tensile crack striking 315°. The double-couple moment tensor is

$$\mathbf{M^{DC}} = \mathbf{M^{CDC}} - \mathbf{M^{tensile}} = \begin{bmatrix} 1 & 0 & 0 \\ 0 & -1 & 0 \\ 0 & 0 & 0 \end{bmatrix} \quad \text{(A17)}$$

This is a 315° striking, vertically dipping left-lateral mechanism.

[51] As is the case for double-couple faulting mechanisms, additional information is required to constrain which of the two possible faulting solutions is the actual one.

A6. Physical Interpretation of CDC Mechanisms

[52] We now wish to consider what subset of all possible moment tensors can be described as the sum of a shear and a tensile crack. In other words, what possible mechanisms are we excluding when we adopt the CDC model? First we note that the deviatoric part of $\mathbf{M}^{\mathbf{tensile}}$ is a compensated linear vector dipole (CLVD) [*Knopoff and Randall*, 1970]. *Knopoff and Randall* [1970] showed that any deviatoric moment tensor can be described as the sum of a double-couple and a CLVD. Therefore the deviatoric part of the CDC moment tensor decomposition is sufficient to represent the deviatoric part of any moment tensor. Also, the restriction in the CDC decomposition is that the trace of the moment tensor is the trace of $\mathbf{M}^{\mathbf{tensile}}$, which is given by

$$\mathrm{tr}\left(\mathbf{M}^{\mathbf{tensile}}\right) = \frac{1+\nu}{\nu} M_C \tag{A18}$$

In general, an arbitrary moment tensor may have any trace. *Dufumier and Rivera* [1997] show that any general moment tensor can be written as

$$\mathbf{M} = \mathbf{M}^{\mathbf{DC}} + \mathbf{M}^{\mathbf{tensile}} + \mathbf{M}^{\mathbf{explosion}} = \mathbf{M}^{\mathbf{CDC}} + \mathbf{M}^{\mathbf{explosion}} \tag{A19}$$

where

$$\mathbf{M}^{\mathbf{explosion}} = \frac{\mathrm{tr}(\mathbf{M}) - \mathrm{tr}\left(\mathbf{M}^{\mathbf{tensile}}\right)}{3}\mathbf{I} \tag{A20}$$

[53] Thus we see that the CDC moment tensor decomposition corresponds to the set of moment tensors where the only isotropic component is that which is associated with an opening fault.

[54] *Dufumier and Rivera* [1997] found several problems with unconstrained full moment tensor (FMT) inversions. Among these is that, when they applied the moment tensor decomposition in equation (A19) to the results of unconstrained FMT inversions, they found that many FMT solutions resulted in large negative explosive components as well as even larger positive tensile components. This means that moment tensors which might appear to have a reasonable volume change actually result from the trade-off between multiple nonphysical volumetric components which compensate each other.

[55] We prefer the CDC source for modeling nondouble-couple volcanic earthquakes because it is based on a physical model of nondouble-couple sources and eliminates the problems associated with full moment tensor inversions.

[56] **Acknowledgments.** Hypocenter information comes from the Japan Meteorological Agency (JMA) with special help from Fumiko Tajima. The EVT7 hypocenter was relocated by Shin'ichi Sakai of the Earthquake Research Institute, University of Tokyo. Geodetic data came from the Geographic Survey Institute of Japan (GSI), and seismic data were provided by the F-net Broadband Seismograph Network. Contribution 9162 of the Caltech Seismological Laboratory.

References

Aki, K., and P. G. Richards (2002), *Quantitative Seismology*, 2nd ed., Univ. Sci. Books, Sausalito, Calif.

Altamimi, Z., P. Sillard, and C. Boucher (2002), A new release of the International Terrestrial Reference Frame for earth science applications, *J. Geophys. Res.*, *107*(B10), 2214, doi:10.1029/2001JB000561.

Apel, E. V., R. Bürgmann, G. Steblov, N. Vasilenko, R. King, and A. Prytkov (2006), Independent active microplate tectonics of northeast Asia from GPS velocities and block modeling, *Geophys. Res. Lett.*, *33*(6), L11303, doi:10.1029/2006GL026077.

Beutler, G., I. I. Mueller, and R. E. Neilan (1994), The International GPS Service for Geodynamics (IGS): Development and start of official service on January 1, 1994, *Bull. Geod.*, *68*(1), 39–70.

Bürgmann, R., P. Segall, M. Lisowski, and J. Svarc (1997), Postseismic strain following the 1989 Loma Prieta earthquake from GPS and leveling measurements, *J. Geophys. Res.*, *102*, 4933–4955.

Choi, K., A. Bilich, K. M. Larson, and P. Axelrad (2004), Modified sidereal filtering: Implications for high-rate GPS positioning, *Geophys. Res. Lett.*, *31*, L22608, doi:10.1029/2004GL021621.

Dreger, D., and B. Woods (2002), Regional distance seismic moment tensors of nuclear explosions, *Tectonophysics*, *356*(1–3), 139–156.

Dreger, D. S., H. Tkalcic, and M. Johnston (2000), Dilational processes accompanying earthquakes in the Long Valley Caldera, *Science*, *288*(5463), 122–125.

Dufumier, H., and L. Rivera (1997), On the resolution of the isotropic component in moment tensor inversion, *Geophys. J. Int.*, *131*(3), 595–606.

Dziewonski, A. M., T.-A. Chou, and J. H. Woodhouse (1981), Determination of earthquake source parameters from waveform data for studies of global regional seismicity, *J. Geophys. Res.*, *86*, 2825–2852.

Fukuyama, E., and D. S. Dreger (2000), Performance test of an automated moment tensor determination system for the future "Tokai" earthquake, *Earth Planets Space*, *52*(6), 383–392.

Furuya, M., S. Okubo, R. Miyajima, I. Meilano, W. Sun, Y. Tanaka, and T. Miyazaki (2003), Mass budget of the magma flow in the 2000 volcano-seismic activity at the Izu-islands, Japan, *Earth Planets Space*, *55*(7), 375–385.

Geshi, N., T. Shimano, T. Chiba, and S. Nakada (2001), Caldera collapse during the 2000 eruption of Miyakejima Volcano, Japan, *Bull. Volcanol.*, *64*(1), 55–68.

Ito, T., and S. Yoshioka (2002), A dike intrusion model in and around Miyakejima, Niijima, and Kozushima in 2000, *Tectonophysics*, *359*(1–2), 171–187.

Japan Meteorological Agency (JMA) (2000), Recent seismic activity in the Miyakejima and Niijima-Kozushima region, Japan—The largest earthquake swarm ever recorded, *Earth Planets Space*, *52*(8), i–vii.

Julian, B. R., and S. A. Sipkin (1985), Earthquake processes in the Long Valley Caldera area, California, *J. Geophys. Res.*, *90*, 11,155–11,169.

Julian, B. R., A. D. Miller, and G. R. Foulger (1997), Non-double-couple earthquake mechanisms at the Hengill-Grensdalur volcanic complex, southwest Iceland, *Geophys. Res. Lett.*, *24*(7), 743–746.

Kanamori, H., G. Ekström, A. Dziewonski, J. S. Barker, and S. A. Sipkin (1993), Seismic radiation by magma injection: An anomalous seismic event near Tori Shima, Japan, *J. Geophys. Res.*, *98*, 6511–6522.

Kikuchi, M., Y. Yamanaka, and K. Koketsu (2001), Source process of the long-period seismic pulses associated with the 2000 eruption of Miyake-Jima Volcano, Japan, and its implications, *J. Geogr.*, *110*(2), 204–216.

Knopoff, L., and M. J. Randall (1970), The compensated linear vector dipole: A possible mechanism for deep earthquakes, *J. Geophys. Res.*, *75*, 4957–4963.

Larson, K., J. Plumb, J. Zwally, and W. Abdalati (2002), Analysis of GPS data collected on the Greenland Ice Sheet, *Pol. Geogr.*, *25*(1), 22–40.

Larson, K. M., A. Bilich, and P. Axelrad (2007), Improving the precision of high-rate GPS, *J. Geophys. Res.*, *112*, B05422, doi:10.1029/2006JB004367.

Lichten, S. M., and J. S. Border (1987), Strategies for high-precision global positioning system orbit determination, *J. Geophys. Res.*, *92*, 12,751–12,762.

Mansinha, L., and D. E. Smylie (1971), The displacement fields of inclined faults, *Bull. Seismol. Soc. Am.*, *61*(5), 1433–1440.

Nakada, S., M. Nagai, A. Yasuda, T. Shimano, N. Geshi, G. Nobuo, M. Ohno, T. Akimasa, T. Kaneko, and T. Fujii (2001), Chronology of the Miyake-Jima 2000 eruption; characteristics of summit collapsed crater and eruption products, *J. Geogr.*, *110*(2), 168–180.

Nishimura, T., S. Ozawa, M. Murakami, T. Sagiya, T. Tada, M. Kaidzu, and M. Ukawa (2001), Crustal deformation caused by magma migration in the northern Izu Islands, Japan, *Geophys. Res. Lett.*, *28*(19), 3745–3748.

Okada, Y. (1985), Surface deformation due to shear and tensile faults in a half-space, *Bull. Seismol. Soc. Am.*, *75*(4), 1135–1154.

Ozawa, S., S. Miyazaki, T. Nishimura, M. Murakami, M. Kaidzu, T. Imakiire, and X. Ji (2004), Creep, dike intrusion, and magma chamber deflation model for the 2000 Miyake eruption and the Izu islands earthquakes, *J. Geophys. Res.*, *109*, B02410, doi:10.1029/2003JB002601.

Saikia, C. K. (1994), Modified frequency-wavenumber algorithm for regional seismograms using Filon's quadrature: Modelling Lg waves in eastern North America, *Geophys. J. Int.*, *118*(1), 142–158.

Seno, T., S. Stein, and A. Gripp (1993), A model for the motion of the Philippine Sea plate consistent with NUVEL-1 and geological data, *J. Geophys. Res.*, *98*, 17,941–17,948.

Templeton, D. C., and D. S. Dreger (2006), Non-double-couple earthquakes in the Long Valley volcanic region, *Bull. Seismol. Soc. Am.*, *96*(1), 69–79, doi:10.1785/0120040206.

Toda, S., R. S. Stein, and T. Sagiya (2002), Evidence from the AD 2000 Izu Islands earthquake swarm that stressing rate governs seismicity, *Nature*, *419*(6902), 58–61.

Zang, S. X., Q. Y. Chen, J. Y. Ning, Z. K. Shen, and Y. G. Liu (2002), Motion of the Philippine Sea plate consistent with the NUVEL-1A model, *Geophys. J. Int.*, *150*(3), 809–819.

R. Bürgmann, Department of Earth and Planetary Science, University of California, 389 McCone Hall 4767, Berkeley, CA 94720-4767, USA. (burgmann@seismo.berkeley.edu)

D. S. Dreger, Department of Geology and Geophysics, 281 McCone Hall, University of California, Berkeley, CA 94720, USA. (dreger@seismo.berkeley.edu)

H. Kanamori, Seismological Laboratory, California Institute of Technology, Pasadena, CA 91125, USA. (hiroo@gps.caltech.edu)

K. M. Larson, Department of Aerospace Engineering Sciences, UCB 429, University of Colorado, Boulder, CO 80309-0429, USA. (kristinem.larson@gmail.com)

S. E. Minson, Department of Geological and Planetary Sciences, California Institute of Technology, 1200 E. California Blvd., MS 252-21, Pasadena, CA 91125-2100, USA. (minson@gps.caltech.edu)